https://dx.doi.org/10.1016/j.engstruct.2020.111291

Two-step translation method for time-dependent reliability of structures subject to both continuous deterioration and sudden events

Hong-Yuan Guo,[1,2,3] You Dong,[3] and Xiang-Lin Gu[1,2,*]

1. Key Laboratory of Performance Evolution and Control for Engineering Structures of Ministry of Education, Tongji University, 1239 Siping Rd., Shanghai 200092, China
2. Department of Structural Engineering, College of Civil Engineering, Tongji University, 1239 Siping Rd., Shanghai 200092, China.
3. Department of Civil and Environmental Engineering, Hong Kong Polytechnic University, Hong Kong 999077, China

Abstract: Civil infrastructure can be subjected to different deterioration scenarios (e.g., continuous deterioration and sudden events) during its service life. Time-dependent reliability analysis of a deteriorating system is of vital importance in the structural design, assessment, and management process. In this paper, a general and novel probability density function-informed framework for time-dependent reliability analysis is developed, considering different deterioration processes and system-level performance. Both continuous deterioration and sudden events are considered within the proposed framework. For the scenario with random sudden drops and/or significant differences in deterioration rates, a novel two-step translation method is proposed to assess the probability density of the performance function within the service life of a structure. In this method, translation operation is conducted twice; the first time to build a virtual and differentiable performance function, and the second, to solve the actual probability density function based on the results from the first step. Then, three illustrative examples are assessed: a simple deteriorating case, a component-level case, and a system-level case. The relevant results demonstrate the feasibility and efficiency of the proposed method.

Keywords: Time-dependent reliability; deteriorating modelling; probability density function-informed method (PDFM); continuous deterioration; sudden event.

* **Corresponding Author**
E-mail address: gxl@tongji.edu.cn
Tel.: +86 21 65982928; fax: +86 21 65982928

1. Introduction

Structural damage generally refers to the changes associated with the geometry and mechanical properties of a structural component or integrated system, which may cause structural performance degradation and affect long-term performance and functionality. During its service life, a structure often suffers from structural deterioration caused by erosion (e.g., chloride ingress, freeze-thaw damage, and concrete carbonation) and hazards (e.g., earthquakes and hurricanes) [1,2] Generally, deterioration scenarios can be divided into two types: continuous deterioration [3–10] and sudden events [11–14]. Continuous deterioration, during the long-term use of a structure, may produce a certain degree of cumulative damage and degradation. A sudden event may result in structural loss of function and even endanger structural safety. Ignoring the relevant single and multiple deteriorations may overestimate the safety and service life of civil infrastructure. Thus, it is of great importance to develop a comprehensive framework for time-dependent reliability assessment by systematically considering different deterioration scenarios.

Within time-dependent performance assessments of deteriorating structures, there are uncertainties associated with structural resistance (e.g., material properties and geometrical characteristics), the occurrence of deterioration scenarios/hazards (e.g., corrosion, earthquakes), operating conditions, and loading cases. Due to these uncertainties, a probabilistic approach is needed for performance assessment. In general, life-cycle performance assessment of a deteriorating structure can be divided into the following categories: state-based assessment, reliability-informed, and renewal theory-based assessment. State-based assessment usually refers to the evaluation of the condition and index of a structure based on inspection [15,16]. For instance, Frangopol and Das [17] proposed the Markovian theory-based approach to conduct a state-based assessment for bridges. However, the residual loading capacity and external load effect could not be identified within this process. Thus, reliability-informed assessment was developed to comprehensively consider the condition and safety changes in the life-cycle of a deterioration process, which became one of the most widely used methods in performance engineering.

Studies have been conducted on developing approaches for reliability analysis (e.g., first-order second-moment method (FOSM) [4], time-series method [18], first-passage method [19,20], and Monte Carlo simulation (MCS) [21–23]). The former two methods aim to calculate the time-dependent reliability based on the probabilistic moments of target functions, while the latter two methods focus on the computation of time-dependent failure probability. For example, Kamiński [18] supposed a time series with Gaussian random coefficients and described a deteriorating system through high order moments. Most of the existing reliability-based assessment approaches focus on the single failure mode associated with reliability analysis [3,24], except for a few studies. Zhang *et al.* [23] studied different failure modes of reinforced concrete (RC) beams, i.e., flexural failure and bond failure on the reliability analysis of corroded RC beams. Furthermore, Bastidas *et al.* [25] developed an analytical framework for the coupling corrosion-fatigue deterioration of RC structures. Additionally, due to the diversities and complexities of failure modes and deterioration mechanisms for components in a structural system, only component-level reliability analysis is inadequate, and system-level reliability analysis should be conducted. For instance, Stewart and Al-Harthy [21] conducted a reliability analysis of a series system for corroded RC beams considering the spatial effect caused by pitting corrosion. By using random field modeling, Tran *et al.* [26] evaluated series system reliability for deteriorating RC bridges suffering from different erosion environments.

Some of the existing studies focus on specific deterioration scenarios and even fewer have incorporated different mechanisms into time-dependent reliability analysis [27]. Thus, a general approach is still needed to incorporate different deterioration scenarios and mechanisms. To achieve such a target, renewal theory-based assessment has recently been employed to assess the life-cycle performance of deteriorating structures, which could take both continuous deterioration and sudden events into consideration. For instance, Yang and Frangopol [28] proposed a life-cycle assessment approach for civil infrastructure under continuous deterioration and hazards. Jia and Gardoni [29] adopted the renewal theory to analyze the time-dependent failure probability of an RC bridge subjected to corrosion and earthquakes. Although the renewal theory-based approach can reveal the random properties of different deterioration

scenarios, such a method focuses on stochastic models rather than the physical nature of deterioration processes and their combination effects. For complex scenarios, it is still necessary to use MCS to capture probabilistic information about target variables, which can be computationally burdensome [2]. Thus, it is of great significance to develop a novel and general method for time-dependent reliability analysis.

In this paper, a general reliability-informed analysis framework is proposed by considering various failure modes, system-level reliability, different deterioration scenarios, and physical mechanisms. A novel probability density function (PDF)-informed method (i.e., PDFM) is proposed to compute the system-level time-dependent reliability of a deteriorating structure under different deterioration scenarios in a unified and comprehensive manner. Section 2 of the paper introduces the proposed general framework for time-dependent reliability analysis under both continuous deterioration and sudden events. The reliability of a deteriorating structure is computed based on the PDF of performance function by solving the general density evolution equation (GDEE). In Section 3, a novel approach is proposed to solve GDEE under different deterioration scenarios. Section 4 presents the application and verification of the proposed framework. MCS is employed to verify the results from the proposed method. Finally, conclusions are drawn and further work is noted.

2. Time-dependent deterioration process and PDF-informed reliability analysis

2.1. General time-dependent deterioration process and reliability analysis

A general performance function of a deteriorating structure can be written as

$$g = G(\boldsymbol{\Theta}, t, \boldsymbol{b}) \tag{1}$$

where t is the time parameter, $\boldsymbol{\Theta} = [\boldsymbol{\Theta}_1, \boldsymbol{\Theta}_2, \ldots, \boldsymbol{\Theta}_d]^{\mathrm{T}}$ is a random vector with d-elements representing all input variables, and $\boldsymbol{b} = \{b_k, k = 1, 2, \ldots, n_{\mathrm{d}}\}$ is a mark vector containing n_{d} critical time instants, in which n_{d} and b_{k} are random variables. The critical time instants refer to the combination of various deterioration mechanisms or the occurrence of a sudden event (e.g., sudden damage and enhancement), which may cause a discontinuity in the $G(\boldsymbol{\Theta}, t, \boldsymbol{b})$ or its derivative function $\dot{G}\left(\boldsymbol{\Theta}, t, \boldsymbol{b}\right)$. For instance, the failure mode of a deteriorating structure may

change from ductile to brittle failure at random time instants [30]. However, structural performance may be enhanced after the application of repair actions [31] and because sudden events occur at random critical time instants, the deterioration rate may be affected. For example, RC structures that have just undergone seismic damage are more susceptible to the ingression of chlorides and rainwater. As a result, the performance function may need to be updated. The introduction of $\boldsymbol{b}$ could incorporate various deterioration processes within the time-dependent performance assessment process. In this paper, the establishment of vector $\boldsymbol{b}$ is related to the changing rate of performance function, and its detailed processes are introduced in section 2.3.2.

In this paper, two types of deterioration modes are considered: continuous deterioration and sudden events. There are two categories of continuous deterioration: Type I and II. Type I refers to differentiable deterioration, where $G(\boldsymbol{\Theta}, t, \boldsymbol{b})$ is derivative subjected to t, and its derivative function, $\dot{G}\left(\boldsymbol{\Theta},t,\boldsymbol{b}\right)$, denotes the rate of performance change due to the deterioration process. Considering the unpredictable change of failure mode caused by a complex deterioration mechanism [5,32], $G(\boldsymbol{\Theta}, t, \boldsymbol{b})$ may remain continuous but $\dot{G}\left(\boldsymbol{\Theta},t,\boldsymbol{b}\right)$ may become discontinuous at time instants $\boldsymbol{b}$, which is called Type II continuous deterioration. Furthermore, considering hazards (e.g. earthquakes and hurricanes) [2,28] and repair actions [13], $G(\boldsymbol{\Theta}, t, \boldsymbol{b})$ may undergo sudden events and $\dot{G}\left(\boldsymbol{\Theta},t,\boldsymbol{b}\right)$ may become infinity at the time instants $\boldsymbol{b}$. Both Type II continuous deterioration and sudden events refer to non-differentiable deterioration. A schematic of three deterioration modes is indicated in Fig. 1, where the PDFs are for illustrative purposes. Fig. 1a presents some samples of $G(\boldsymbol{\Theta}, t, \boldsymbol{b})$ without repair actions, associated with the three deterioration modes (two samples for each deterioration mode), while Fig. 1b shows the samples of $G(\boldsymbol{\Theta}, t, \boldsymbol{b})$ of sudden events with repair actions, where performance function would be enhanced after repair actions.

Within a service life, the number of critical time instants is random and three deterioration modes could exist, which may form a mixture of deterioration. The introduction of $\boldsymbol{b}$ facilitates considering multiple deterioration processes within the performance assessment process and acts as a contribution to the proposed formulation of life-cycle performance.

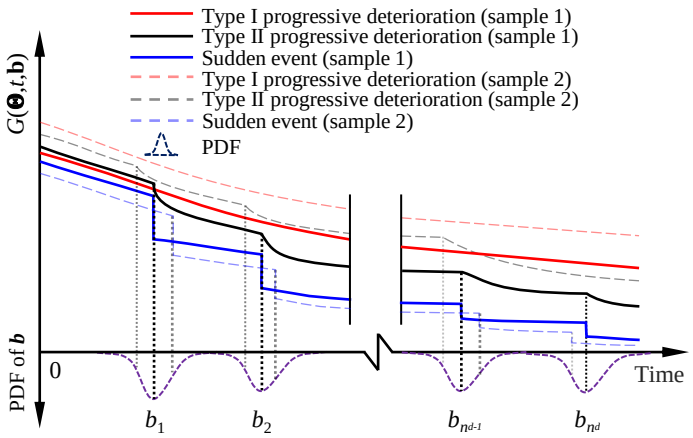

(a)

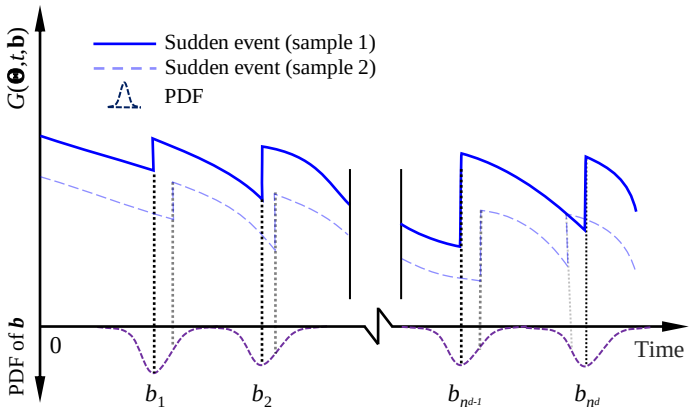

(b)

Fig. 1. Performance function $G(\boldsymbol{\Theta}, t, \boldsymbol{b})$ under different deterioration scenarios: (a) without repair actions and (b) with repair actions

For system reliability analysis, the systematic performance function needs to be established based on the performance function of each component. For instance, the performance function, $G(\boldsymbol{\Theta}, t, \boldsymbol{b})$, of a series system can be denoted as an equivalent value event, as shown in Eq.(2) [33].

$$g = G(\boldsymbol{\Theta}, t, \boldsymbol{b}) = \min_{i=1}^{m} G_i(\boldsymbol{\Theta}, t, \boldsymbol{b}) \tag{2}$$

where $G_i(\boldsymbol{\Theta}, t, \boldsymbol{b})$ is the performance function of the i-th component (i=1, 2, …., m) and $\min_{i=1}^{m}(\cdot)$ denotes the minimum value among m performance functions. For a parallel system, the function in Eq.(2) could be replaced by $\max_{i=1}^{m}(\cdot)$ to obtain the maximum value amongst m performance functions [33]. In practical engineering, there is also a mixed system containing both series and

parallel subsystems. If only the performance function, $G(\boldsymbol{\Theta}, t, \boldsymbol{b})$, of the system is expressed, the proposed framework can be conducted.

A structure would reach its limit state once $G(\boldsymbol{\Theta}, t, \boldsymbol{b})$ is equal to or below zero. The time-dependent failure probability, $p_f(t)$, depends on prior performance history rather than instantaneous performance. The $p_f(t)$ can be computed as [34]

$$p_f(t) = 1 - \Pr\left[\bigcap_{t_k, k=1,2,\ldots,n} G(\boldsymbol{\Theta}, t_k, \boldsymbol{b}) > 0\right] \tag{3}$$

where t_k (k = 1, 2, …, n) is a discrete-time instant. Considering the continuity of time t, Eq.(3) can be rewritten as

$$p_f(t) = 1 - \Pr\{G(\boldsymbol{\Theta}, \tau, \boldsymbol{b}) > 0,\ 0 \le \tau \le t\} \tag{4}$$

Eq.(4) could be solved using MCS. However, this is a time-consuming and inefficient method that requires a prohibitive computational effort to obtain high accuracy, especially for a small probability and high-dimensional problem. Therefore, a means of improving the sampling efficiency was proposed, such as low-discrepancy sequences (e.g., Sobol sequence) [35], Latin Hypercube sampling [36, 37], and importance sampling [38], among others.

In this paper, $p_f(t)$ will be calculated based on the PDF of performance function $p_G(g, t)$, which can be called PDFM. To consider the first-passage problem, an absorbing boundary condition is given as

$$p_G(g,t)|_{g<0} = 0 \tag{5}$$

, which is used to obtain residual PDF, $p^*_G(g, t)$. Meanwhile, $p_f(t)$ can be acquired by

$$p_f(t) = 1 - \int_0^{+\infty} p_G^*(g,t)\mathrm{d}g \tag{6}$$

To compute $p_f(t)$, it is important to obtain the PDFs of performance function under different types of deterioration modes, which will be discussed in the following section.

2.2. PDFM for Type I continuous deterioration

To facilitate the application of the proposed framework, the computational methods of PDFM associated with time-dependent reliability analysis considering different deterioration processes are discussed in this section. To begin with, the PDFM for Type I continuous deterioration

(differentiable deterioration) is reviewed because relevant algorithms have already been studied [39, 40]. However, there are a lack of approaches for achieving PDFM under non-differentiable deterioration scenarios, i.e., Type II continuous deterioration and sudden events. Accordingly, methods are proposed to compute time-dependent reliability by incorporating different deterioration processes in a unified manner.

For differentiable deterioration, the PDF of performance function can be solved using existing algorithms of PDFM. Without the vector of critical time instant $\boldsymbol{b}$, $G(\boldsymbol{\Theta}, t, \boldsymbol{b})$ can be written as $G(\boldsymbol{\Theta}, t)$, which is differentiable subjected to t, i.e., $\dot{G}(\boldsymbol{\Theta}, t)$. Furthermore, denoting the joint probability density of $G(\boldsymbol{\Theta}, t)$ and $\boldsymbol{\Theta}$, as $p_{G\boldsymbol{\Theta}}(g, \boldsymbol{\theta}, t)$, based on the principle of probability preservation, the integration of $p_{G\boldsymbol{\Theta}}(g, \boldsymbol{\theta}, t)$ within an arbitrary augmented domain, $\Omega_t \times \Omega_{\boldsymbol{\Theta}}$, remains unchanged with time [40].

$$
\begin{aligned}
&\frac{\mathrm{d}}{\mathrm{d}t}\left\{\int_{\Omega_t\times\Omega_\Theta} p_{G\Theta}(g,\boldsymbol{\theta},t)\mathrm{d}g\mathrm{d}\boldsymbol{\theta}\right\} = \frac{\mathrm{d}}{\mathrm{d}t}\left\{\int_{\Omega_0\times\Omega_\Theta} p_{G\Theta}(g,\boldsymbol{\theta},t)\left|J\right|\mathrm{d}g\mathrm{d}\boldsymbol{\theta}\right\} \\
&= \int_{\Omega_0\times\Omega_\Theta}\left\{\frac{\partial p_{G\Theta}(g,\boldsymbol{\theta},t)}{\partial t} + \dot{G}(\boldsymbol{\Theta},t)\frac{\partial p_{G\Theta}(g,\boldsymbol{\theta},t)}{\partial g}\right\}\left|J\right|\mathrm{d}g\mathrm{d}\boldsymbol{\theta} \\
&= \int_{\Omega_t\times\Omega_\Theta}\left\{\frac{\partial p_{G\Theta}(g,\boldsymbol{\theta},t)}{\partial t} + \dot{G}(\boldsymbol{\Theta},t)\frac{\partial p_{G\Theta}(g,\boldsymbol{\theta},t)}{\partial g}\right\}\mathrm{d}g\mathrm{d}\boldsymbol{\theta} = 0
\end{aligned}
\tag{7}
$$

where Ω_0 denotes the time domain when $t = 0$; J and $\mathrm{d}\{\cdot\}/\mathrm{d}t$ refer to the Jacobian matrix and the total derivative, respectively.

Due to the arbitrariness of Ω_t and Ω_Θ, removing its integral sign in Eq.(7), a partial differential equation could be obtained:

$$
\frac{\partial p_{G\Theta}(g,\boldsymbol{\theta},t)}{\partial t} + \dot{G}(\boldsymbol{\Theta},t)\frac{\partial p_{G\Theta}(g,\boldsymbol{\theta},t)}{\partial g} = 0 \tag{8}
$$

This is known as the generalized density evolution equation (GDEE) [39], which is similar to the Liouville equation [41] or Dosupov-Pugachev equation [41] as follows

$$
\frac{\partial p_{G\Theta}(g,\boldsymbol{\theta},t)}{\partial t} + \frac{\partial\left[p_{G\Theta}(g,\boldsymbol{\theta},t)\cdot G(\boldsymbol{\Theta},t)\right]}{\partial g} = 0 \tag{9}
$$

However, compared with Eq.(9), $G(\boldsymbol{\Theta}, t)$ and $p_{G\boldsymbol{\Theta}}(g, \boldsymbol{\theta}, t)$ in Eq.(8) are decoupled and can be solved easier. The boundary condition and analytical solution are as follows

$$
p_{G\Theta}(g,\boldsymbol{\theta},0) = \delta[g - G(\boldsymbol{\Theta},0)]p_{\boldsymbol{\Theta}}(\boldsymbol{\theta}) \tag{10}
$$

$$p_{G\Theta}(g,\boldsymbol{\theta},t)=\delta[g-G(\boldsymbol{\Theta},t)]p_{\boldsymbol{\Theta}}(\boldsymbol{\theta}) \tag{11}$$

where $\delta(\cdot)$ is the Dirac's delta function, and $p_{\boldsymbol{\Theta}}(\boldsymbol{\theta})$ is the joint PDF of $\boldsymbol{\Theta}$.

Although closed-form solutions might be obtained in some specific scenarios of GDEE, numerical solutions are more common than closed-form solutions in most cases [42]. In this study, the finite difference method (FDM) and point evolution method developed by Li *et al.* [39] are employed to solve GDEE and more detailed information is presented in Appendix A.1.

Once the solution of GDEE, $p_{G\boldsymbol{\Theta}}(g, \boldsymbol{\theta}, t)$, is obtained, the PDF of $G(\boldsymbol{\Theta}, t)$, that is, $p_G(g,t)$, can be calculated as

$$p_G(g,t)=\int_{\Omega_{\boldsymbol{\Theta}}} p_{G\boldsymbol{\Theta}}(g,\boldsymbol{\theta},t)\,\mathrm{d}\boldsymbol{\theta}=\int_{\Omega_{\boldsymbol{\Theta}}}\delta\left[g-G(\boldsymbol{\Theta},t)\right]p_{\boldsymbol{\Theta}}(\boldsymbol{\theta})\,\mathrm{d}\boldsymbol{\theta} \tag{12}$$

Additionally, Eq.(5) needs to be imposed to consider the first-passage problem. According to the point evolution method and Eqs.(8), (10)–(12), $p_G^*(g,t)$ could be obtained and then $p_f(t)$ can be computed using Eq.(6).

2.3. PDFM for Type II continuous deterioration and sudden events

For a deterioration model with sudden events or Type II continuous deterioration, $\dot{G}\left(\boldsymbol{\Theta},t,\boldsymbol{b}\right)$ might be infinity or discontinuous in some time instants. Both situations could be called non-differentiable deterioration. Two main issues exist in conducting PDFM for non-differentiable deterioration: (1) identifying vector $\boldsymbol{b}$ of critical time instants; (2) solving GDEE for a non-differentiable performance function. In this study, vector $\boldsymbol{b}$ is regarded as the output of the deterioration system and could be identified by analyzing performance function versus time. Given an input vector, $\boldsymbol{\theta}$, a sample of performance function, $G(\boldsymbol{\theta}, t, \boldsymbol{b})$, could be obtained and then $\boldsymbol{b}$ could be captured by the time instants of the infinite and discontinuous derivative function $\dot{G}\left(\boldsymbol{\theta},t,\boldsymbol{b}\right)$. For instance, in Fig. 1, given input vector $\boldsymbol{\theta}$, the number n_d and time instants of sudden events or deterioration rate, changes could be identified, and $\boldsymbol{b}$ becomes a deterministic vector. Then, $G(\boldsymbol{\theta}, t, \boldsymbol{b})$ could be expressed using a piecewise function

$$\begin{aligned} g&=G\left(\boldsymbol{\theta},t,\boldsymbol{b}\right)\\ &=g_1\cdot\left[1-H\left(t-b_1\right)\right]+\sum_{s=2}^{n_d}g_s\cdot\left[1-H\left(t-b_s\right)\right]\cdot H\left(t-b_{s-1}\right)+g_{n_d+1}\cdot H\left(t-b_{n_d}\right)\end{aligned} \tag{13}$$

where, $H(x)$ is the Heaviside function and equals 1 when $x \geq 0$ and 0 when $x < 0$, g_s denotes the performance function curve at different stages (i.e., g_1, g_{n_d+1}, and g_s ($1< s <n_d+1$) denotes the $G(\boldsymbol{\theta}, t, \boldsymbol{b})$ within $[0, b_1)$, $[b_{n_d}, +\infty)$, and $[b_{s-1}, b_s)$, respectively). Then, the derivative function of Eq.(13) can be written as

$$\begin{aligned}\dot{g} = \dot{G}(\boldsymbol{\theta},t,\boldsymbol{b}) &= \dot{g}_1 \cdot \left[1-H\left(t-b_1\right)\right] - g_1 \cdot \delta\left(t-b_1\right) \\ &+\dot{g}_2 \cdot \left[1-H\left(t-b_2\right)\right] \cdot H\left(t-b_1\right) - g_2 \cdot \delta\left(t-b_2\right) \cdot H\left(t-b_1\right) + g_2 \cdot \left[1-H\left(t-b_2\right)\right] \cdot \delta\left(t-b_1\right) \\ &+\sum_{s=3}^{n_d} \left\{ \begin{array}{l} \dot{g}_s \cdot \left[1-H\left(t-b_s\right)\right] \cdot H\left(t-b_{s-1}\right) - g_s \cdot \delta\left(t-b_s\right) \cdot H\left(t-b_{s-1}\right) \\ +g_s \cdot \left[1-H\left(t-b_s\right)\right] \cdot \delta\left(t-b_{s-1}\right) \end{array} \right\} \\ &+\dot{g}_{n_d+1} \cdot H(t-b_{n_d}) + g_{n_d+1} \cdot \delta\left(t-b_{n_d}\right)\end{aligned} \tag{14}$$

where $\dot{g}_s$, $s = 1, 2, \ldots$and $n_d + 1$ is the derivative of g_s. Due to the existence of Dirac's delta function $\delta(\cdot)$ in Eq.(14), its GDEE may not be obtained directly. If the critical time instants are deterministic, such a GDEE could be easily established and solved by a piecewise GDEE [43]. However, in general, critical time instants are random variables, and a piecewise GDEE is not easily established. Thus, to solve such an issue, two approaches are proposed: approximate changing rate method and two-step translation method.

2.3.1. Approximate changing rate method

To solve the discontinuous issue for the derivative function of performance function (i.e., the left side derivative does not agree with the right side derivative at a local time instant), a discrete surrogate function, $Y(t)$, and its differentiable function, $\dot{Y}(t)$, under a given input random vector, $\boldsymbol{\theta}$, and time step, Δt, is created as follows

$$Y(t) = G(\boldsymbol{\theta}, k\cdot\Delta t, \boldsymbol{b}),\ k = 0,1,2,\ldots,n_t \tag{15}$$

$$\dot{Y}(t) = \begin{cases} \dfrac{G\left(\boldsymbol{\theta},\left(k+1\right)\cdot\Delta t,\boldsymbol{b}\right) - G\left(\boldsymbol{\theta},k\cdot\Delta t,\boldsymbol{b}\right)}{\Delta t}, k = 0 \\ \dfrac{G\left(\boldsymbol{\theta},\left(k+1\right)\cdot\Delta t,\boldsymbol{b}\right) - G\left(\boldsymbol{\theta},\left(k-1\right)\cdot\Delta t,\boldsymbol{b}\right)}{2\Delta t}, k = 1,2,\ldots,n_t-1 \\ \dfrac{G\left(\boldsymbol{\theta},k\cdot\Delta t,\boldsymbol{b}\right) - G\left(\boldsymbol{\theta},\left(k-1\right)\cdot\Delta t,\boldsymbol{b}\right)}{\Delta t}, k = n_t \end{cases} \tag{16}$$

Then, denoting the joint PDF of ($Y(t)$, $\boldsymbol{\theta}$, $\boldsymbol{b}$) as $p_{Y\boldsymbol{\Theta B}}(y, \boldsymbol{\theta}, t, \boldsymbol{b})$, the GDEE of $Y(t)$ can be obtained

$$\frac{\partial p_{Y\boldsymbol{\Theta B}}(y,\boldsymbol{\theta},t,\boldsymbol{b})}{\partial t} = -\dot{Y}(t)\frac{\partial p_{Y\boldsymbol{\Theta B}}(y,\boldsymbol{\theta},t,\boldsymbol{b})}{\partial y} \tag{17}$$

which is similar to Eq.(8), and the PDF of $Y(t)$ can also be obtained by the point evolution method and FDM (Appendix A.1). In this method, the GDEE of non-differentiable deterioration is treated as that of differentiable deterioration, and vector $\boldsymbol{b}$ of critical time instants does not need to be identified.

However, to achieve of FDM, the parameters of the finite-difference grid, i.e., time step Δt and space step Δx, need to be determined and subjected to the restriction of the Courant–Friedrichs–Lewy (CFL) [44] condition in Eq.(18):

$$\left|\frac{\Delta t}{\Delta f} v\right| \le 1 \tag{18}$$

where v is the velocity of the sampled performance function referring to Eq.(46). Regarding the CFL condition, space step Δx must be not less than $v \cdot \Delta t$, which means that v could limit the selection of Δx and Δt. Thus, the "approximate changing rate method" may not work well with a case with dramatic changes of $G(\boldsymbol{\Theta}, t, \boldsymbol{b})$, as $\dot{G}(\boldsymbol{\Theta},t,\boldsymbol{b})$ would limit the choice of space step Δx.

2.3.2. Proposed two-step translation method

The principal idea of the "two-step translation method" is to establish a virtual and differentiable performance function, $\tilde{G}(\boldsymbol{\theta},t,\boldsymbol{b})$, in terms of $G(\boldsymbol{\theta}, t, \boldsymbol{b})$ and then obtain the PDF of $G(\boldsymbol{\theta}, t, \boldsymbol{b})$ based on the PDF of $\tilde{G}(\boldsymbol{\theta},t,\boldsymbol{b})$ indirectly. Removing the $\delta(\cdot)$ in the differentiable function of $G(\boldsymbol{\theta}, t, \boldsymbol{b})$ in Eq.(14), the differentiable function of $\tilde{G}(\boldsymbol{\theta},t,\boldsymbol{b})$, $\dot{\tilde{G}}(\boldsymbol{\theta},t,\boldsymbol{b})$, could be written as

$$
\begin{aligned}
\dot{\tilde{G}}(\boldsymbol{\theta},t,\mathbf{b}) &= \dot{g}_1\cdot\left[1-H\left(t-b_1\right)\right]+\dot{g}_2\cdot\left[1-H(t-b_2)\right]\cdot H(t-b_1)\\
&+\sum_{s=3}^{n_d}\dot{g}_s\cdot\left[1-H\left(t-b_s\right)\right]\cdot H\left(t-b_{s-1}\right)+\dot{g}_{n_d+1}\cdot H(t-b_{n_d})\\
&= \dot{G}\left(\boldsymbol{\theta},t,\mathbf{b}\right)-\left\{g_2\cdot\left[1-H\left(t-b_2\right)\right]-g_1\right\}\cdot\delta\left(t-b_1\right)\\
&-\sum_{s=2}^{n_d-1}\left\{g_{s+1}\cdot\left[1-H\left(t-b_{s+1}\right)\right]-g_s\cdot H\left(t-b_{s-1}\right)\right\}\cdot\delta\left(t-b_s\right)\\
&-\left[g_{n_d+1}-g_{n_d}\cdot H\left(t-b_{n_d-1}\right)\right]\cdot\delta\left(t-b_{n_d}\right)
\end{aligned}
\tag{19}
$$

where $g_{s+1}\cdot\left[1-H\left(t-b_{s+1}\right)\right]-g_s\cdot H\left(t-b_{s-1}\right)$ could be calculated by the difference value of $G(\boldsymbol{\theta}, t, \boldsymbol{b})$ between the time instants immediately before and after b_s, i.e., b_s^- and b_s^+

$$
g_{s+1}\cdot\left[1-H\left(t-b_{s+1}\right)\right]-g_s\cdot H\left(t-b_{s-1}\right)=g_{s+1}(b_s^+)-g_s(b_s^-) \tag{20}
$$

where $g_s(b_s^-)$ and $g_{s+1}(b_s^+)$ denote $G(\boldsymbol{\theta},b_s^-,\boldsymbol{b})$ and $G(\boldsymbol{\theta},b_s^+,\boldsymbol{b})$, respectively. Then, $\dot{\tilde{G}}(\boldsymbol{\theta},t,\boldsymbol{b})$ could be rewritten as Eq.(21)

$$
\dot{\tilde{G}}(\boldsymbol{\theta},t,\boldsymbol{b})=\dot{G}\left(\boldsymbol{\theta},t,\boldsymbol{b}\right)-\sum_{s=1}^{n_d}\left[g_{s+1}(b_s^+)-g_s(b_s^-)\right]\cdot\delta\left(t-b_s\right) \tag{21}
$$

and $\tilde{G}(\boldsymbol{\theta},t,\boldsymbol{b})$ could be obtained as Eq.(22) by integrating Eq.(21)

$$
\tilde{G}(\boldsymbol{\theta},t,\boldsymbol{b})=G(\boldsymbol{\theta},t,\boldsymbol{b})-\sum_{s=1}^{n_d}\left[g_{s+1}(b_s^+)-g_s(b_s^-)\right]\cdot H\left(t-b_s\right) \tag{22}
$$

Denoting the joint density probability of $(\tilde{G},\boldsymbol{\theta},\boldsymbol{b})$ as $p_{\tilde{G}\boldsymbol{\Theta}\mathbf{B}}(g,\boldsymbol{\theta},t,\boldsymbol{b})$, its GDEE could be obtained as in Eq.(17)

$$
\frac{\partial p_{\tilde{G}\boldsymbol{\Theta}\mathbf{B}}(g,\boldsymbol{\theta},t,\boldsymbol{b})}{\partial t}=-\dot{\tilde{G}}(\boldsymbol{\theta},t,\boldsymbol{b})\frac{\partial p_{\tilde{G}\boldsymbol{\Theta}\mathbf{B}}(g,\boldsymbol{\theta},t,\boldsymbol{b})}{\partial g} \tag{23}
$$

The solution of Eq.(23) can be denoted as

$$
p_{\tilde{G}\boldsymbol{\Theta}\mathbf{B}}(g,\boldsymbol{\theta},t,\boldsymbol{b})=\delta\left[g-\tilde{G}(\boldsymbol{\theta},t,\boldsymbol{b})\right]\cdot p_{\boldsymbol{\Theta}}(\boldsymbol{\theta}) \tag{24}
$$

In terms of Eqs.(22) and (24), $p_{G\boldsymbol{\Theta}\mathbf{B}}(g, \boldsymbol{\theta}, t, \boldsymbol{b})$ can be rewritten as

$$
\begin{aligned}
& p_{G\boldsymbol{\Theta}\mathbf{B}}(g,\boldsymbol{\theta},t,\boldsymbol{b}) = \delta\left[g - G\left(\boldsymbol{\theta},t,\boldsymbol{b}\right)\right]\cdot p_{\boldsymbol{\Theta}}\left(\boldsymbol{\theta}\right) \\
& = \delta\left\{g - \sum_{s=1}^{n_d}\left[g_{s+1}(b_s^+) - g_s(b_s^-)\right]\cdot H\left(t-b_s\right) - \tilde{G}\left(\boldsymbol{\theta},t,\boldsymbol{b}\right)\right\}\cdot p_{\boldsymbol{\Theta}}\left(\boldsymbol{\theta}\right) \\
& = p_{\tilde{G}\boldsymbol{\Theta}\mathbf{B}}\left\{g - \sum_{s=1}^{n_d}\left[g_{s+1}(b_s^+) - g_s(b_s^-)\right]\cdot H\left(t-b_s\right),\boldsymbol{\theta},t,\boldsymbol{b}\right\}
\end{aligned}
\tag{25}
$$

Being similar to Eq.(12), $p_G(g,t)$ can be described as

$$
\begin{aligned}
& p_G(g,t) = \int_{D_{\boldsymbol{\Theta}}} p_{G\boldsymbol{\Theta}\mathbf{B}}(g,\boldsymbol{\theta},t,\boldsymbol{b})\ \mathrm{d}\boldsymbol{\theta} \\
& = \int_{D_{\boldsymbol{\Theta}}} p_{\tilde{G}\boldsymbol{\Theta}\mathbf{B}}\left\{g - \sum_{s=1}^{n_d}\left[g_{s+1}(b_s^+) - g_s(b_s^-)\right]\cdot H\left(t-b_s\right),\boldsymbol{\theta},t,\boldsymbol{b}\right\}\mathrm{d}\boldsymbol{\theta} \\
& = \int_{D_{\boldsymbol{\Theta}}} \delta\left\{g - \sum_{s=1}^{n_d}\left[g_{s+1}(b_s^+) - g_s(b_s^-)\right]\cdot H\left(t-b_s\right)\right\} p_{\boldsymbol{\Theta}}(\boldsymbol{\theta})\ \mathrm{d}\boldsymbol{\theta}
\end{aligned}
\tag{26}
$$

As indicated above, GDEE for $G(\boldsymbol{\theta}, t, \boldsymbol{b})$ of discontinuous deterioration can be replaced by solving Eq.(23). The establishment of $\tilde{G}(\boldsymbol{\theta},t,\boldsymbol{b})$ and computation of $p_{G\boldsymbol{\Theta}\mathbf{B}}(g, \boldsymbol{\theta}, t, \boldsymbol{b})$ are in terms of Eqs.(22) and (25), respectively, which are bridge elements translating between the virtual performance function and the PDF of the target performance function. Thus, the proposed method is named the "two-step translation method".

In practical numerical achievement, a discrete surrogate function also needs to be employed. Meanwhile, n_{sel} representative points are acquired in terms of the point evolution method. However, unlike the "approximate changing rate method", the "two-step translation method" is based on the intermediate PDF and the differences between the virtual and actual performance functions. Thus, in practice, the negative effects of sudden events can be diminished, and the selection of finite-difference grids becomes flexible. In theory, the approach presented in this subsection can lead to more accurate computational results than the method presented in section 2.3.1.

Taking one representative point without repair actions as an example, Fig. 2 illustrates the schematics of the proposed method, whose main processes are as follows:

(1) For a given representative point, $\boldsymbol{\theta}_a$, (a = 1, 2, …, n_{sel}), the discrete surrogate model, $Y(k\cdot\Delta t)$ (k = 0,1,2,…,n_t), and its differentiable function, $\dot{Y}(k\cdot\Delta t)$ could be created by Eqs.(15)

and (16), as shown in Fig. 2a. From $k = 1$ to n_t, each $\dot{Y}(k\cdot\Delta t)$ would be compared with $\dot{Y}\left((k-1)\cdot\Delta t\right)$ and the $k\cdot\Delta t$ would be recorded as the critical time instant $b_{a,s} = k_{a,s}\cdot\Delta t$ once $\dot{Y}(k\cdot\Delta t)$ exceeds $\alpha\cdot\dot{Y}\left((k-1)\cdot\Delta t\right)$ (α is a custom index and not less than 1.0). All recorded $b_{a,s}$ could be stored in vector $\boldsymbol{b}_a$ and its length, $n_{a,nd}$, determined by the number of $b_{a,s}$ ($s = 1,2,\ldots,n_{a,nd}$).

(2) Next, the first translation establishes a virtual and differentiable $\tilde{Y}(t)$. For each $b_{a,s}$, the $\{Y(t), t > b_{a,i}\}$ would be translated upwards to form $\tilde{Y}(t)$, i.e., Eq.(27), with a distance Δg_s, i.e., Eq.(28):

$$\tilde{Y}(t) = Y(t) + \Delta g_s \tag{27}$$

$$\Delta g_s = -\left(g_{s+1}(b_{a,s}^{+}) - g_s(b_{a,s}^{-})\right) \approx \left|2Y\left(k_{a,s}\cdot\Delta t\right) - Y\left(\left(k_{a,s}-1\right)\cdot\Delta t\right) - Y\left(\left(k_{a,s}+1\right)\cdot\Delta t\right)\right| \tag{28}$$

where $b_{a,s}^{-}$ and $b_{a,s}^{+}$ are the time instants immediately before and after $b_{a,s}$, respectively, and $g_s(b_{a,s}^{-})$ and $g_{s+1}(b_{a,s}^{+})$ denote $G(\boldsymbol{\theta}, b_s^{-}, \boldsymbol{b}_a)$ and $G(\boldsymbol{\theta}, b_s^{+}, \boldsymbol{b}_a)$, respectively. Steps (1) and (2) can be repeated many times, until no more critical time instants are found. Then, $\tilde{Y}(t)$ could be obtained, as presented in Fig.2a.

(3) Applying the point evolution method (Appendix A.1), the GDEE of $\tilde{Y}(t)$ would be solved to obtain $p_{\tilde{Y}\boldsymbol{\Theta}\boldsymbol{B}}(\tilde{y},\boldsymbol{\theta},t,\boldsymbol{b})$. Then, the second translation could be conducted to obtain $p_{Y\boldsymbol{\Theta}\boldsymbol{B}}(y, \boldsymbol{\theta}, t, \boldsymbol{b})$. As shown in Fig.2b, $p_{\tilde{Y}\boldsymbol{\Theta}\boldsymbol{B}}(\tilde{y},\boldsymbol{\theta},t,\boldsymbol{b})$ would be translated back to $p_{Y\boldsymbol{\Theta}\boldsymbol{B}}(y, \boldsymbol{\theta}, t, \boldsymbol{b})$ by Eq.(29) and $p_Y(y, t)$ could be computed by summarizing all $p_{Y\boldsymbol{\Theta}\boldsymbol{B}}(y, \boldsymbol{\theta}, t, \boldsymbol{b})$ under a given $\boldsymbol{\theta}$ by Eq.(30).

$$p_{Y\boldsymbol{\Theta}\boldsymbol{B}}(y,\boldsymbol{\theta},t,\boldsymbol{b}) = p_{\tilde{Y}\boldsymbol{\Theta}\boldsymbol{B}}\left(y + \sum_{s=1}^{n_d}\Delta g_s\cdot H\left(t-b_s\right),\boldsymbol{\theta},t,\boldsymbol{b}\right) \tag{29}$$

$$p_Y\left(y,t\right) = \int_{D_{\boldsymbol{\Theta}}} p_{Y\boldsymbol{\Theta}\boldsymbol{B}}(y,\boldsymbol{\theta},t,\boldsymbol{b})\,\mathrm{d}\boldsymbol{\theta} = \int_{D_{\boldsymbol{\Theta}}} p_{\tilde{Y}\boldsymbol{\Theta}\boldsymbol{B}}\left(y + \sum_{s=1}^{n_d}\Delta g_s\cdot H\left(t-b_s\right),\boldsymbol{\theta},t,\boldsymbol{b}\right)\mathrm{d}\boldsymbol{\theta} \tag{30}$$

For the scenarios with repair actions, the performance function might increase after the critical time instants, then the direction of arrows in Figs. 2a and b should be reversed.

Based on the proposed method, the non-differentiable deterioration model with sudden events can be solved and its principal processes are presented in Fig. 3. Additionally, regarding the selection of Δt in Eq.(28), a small Δt could increase the accuracy of the computational results but increase the computational burden, whereas a large Δt may decrease the computational accuracy but increase efficiency. In this study, the annual reliability index is investigated and Δt is 0.5 years.

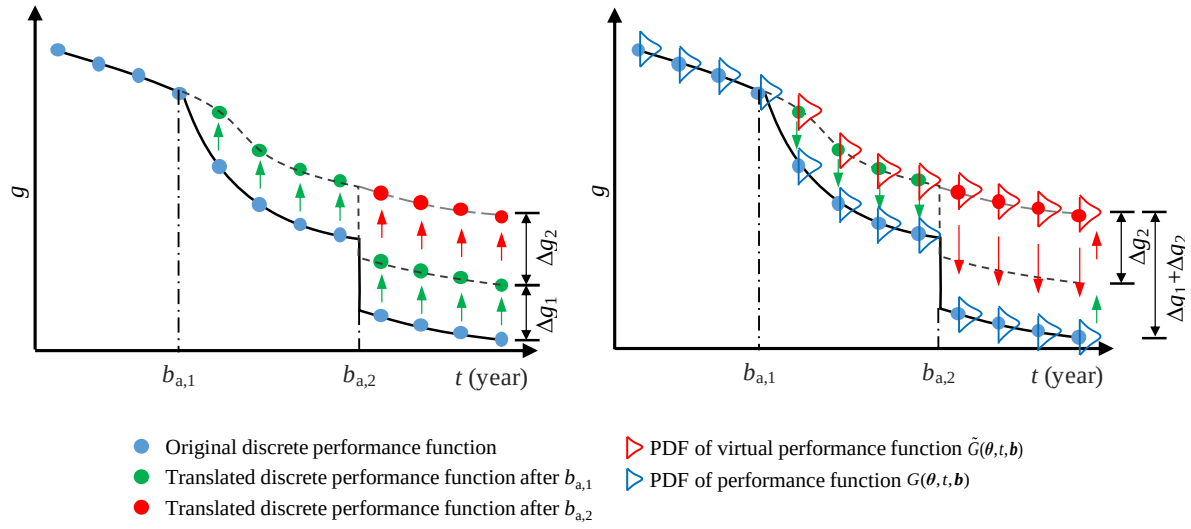

(a) First translation (b) Second translation

Fig. 2. Schematic of the "two-step translation method"

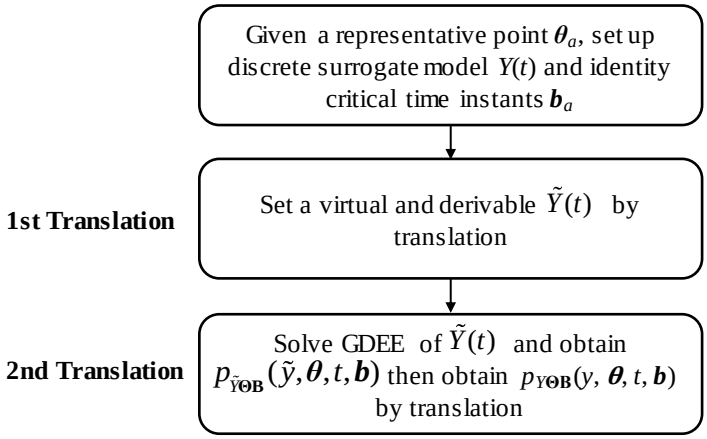

Fig. 3. Computational flowchart of the "two-step translation method"

The PDFM-informed reliability analysis processes for three types of deterioration modes are illustrated in Fig. 4; the steps of establishing the original deterioration model and point selection remain unchanged for each scenario. The "approximate changing rate method" could achieve PDFM for continuous deterioration, and its deterioration rate could be represented by

establishing a simple surrogate model. For the deterioration process with sudden events or high changing deterioration rates, the "approximate changing rate method" may not be suitable, but the "two-step translation method" can be used to solve the issue by applying a translated surrogate model and obtaining the target PDF indirectly. Then, the time-dependent failure probability could be computed by integrating the residual PDF.

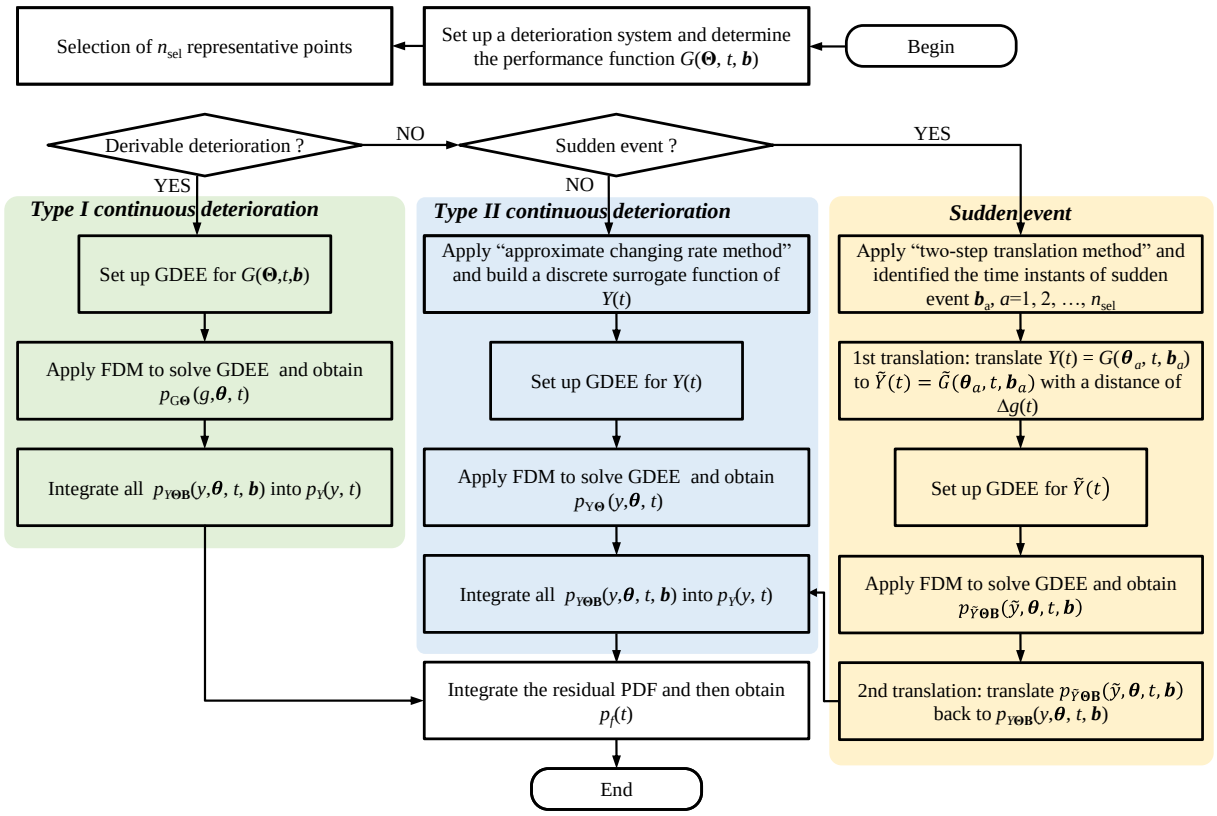

Fig. 4. Time-dependent reliability analysis framework of a deteriorating structure under different scenarios (the green, blue and yellow zones denote the processes for Type I continuous deterioration, Type II continuous deterioration, and sudden events, respectively)

3. Illustrative examples

This section presents three examples to illustrate the feasibility and applicability of the proposed approach. The first investigates time-dependent performance under sudden events. The second focuses on component-level time-dependent reliability analysis considering the integration of different deterioration mechanisms (e.g., deterioration of reinforcement, bond-slip). The final example illustrates the application of the proposed framework to estimate the system-level time-dependent reliability of the deteriorating structure. All examples are coded using CPP and compiled by Visual Studio 2019, with the programs running on Intel (R) Core (TM) i7-

4790CPU@3.6GHz and 24GB of RAM.

3.1. A deteriorating system with sudden events

To demonstrate the efficiency and accuracy of the proposed PDFM considering sudden events, numerical cases are made. Supposing a stochastic deterioration system with one sudden damage at a random time instant t_{drop}

$$f(t) = (1 - 6\times10^{-6}t^3)\cdot f_0 - 5\cdot H(t - t_{drop}) \tag{31}$$

where, both f_0 and t_{drop} are Gaussian random variables ($f_0 \sim N(20,1)$ and $t_{\text{drop}} \sim N(25,2)$). Based on the method in Appendix A.1, 144 representative points are selected to achieve PDFM and Fig. 5 presents the PDF results of the "two-step translation method", where sudden damage occurs within 20–30 years.

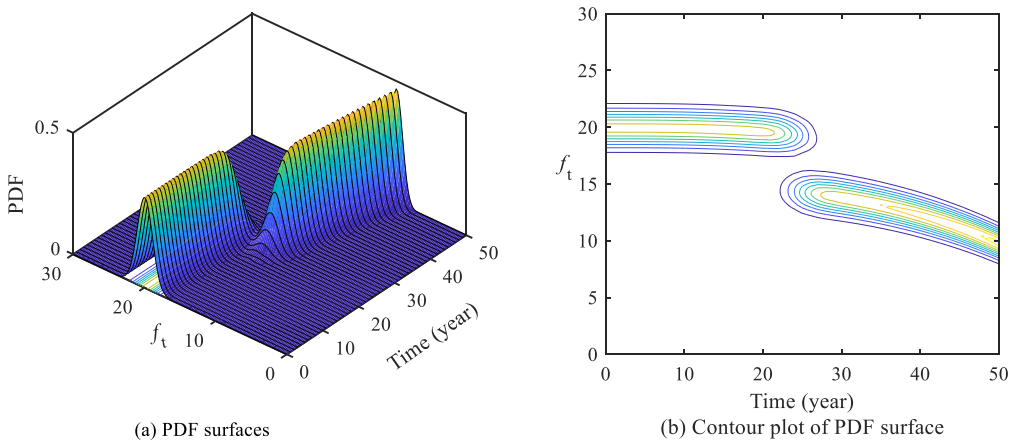

(a) PDF surfaces (b) Contour plot of PDF surface

Fig. 5.PDF results of the "two-step translation method"

Besides, Fig. 6 compares the differences between the "two-step translation method" and the "approximate velocity method" by the PDF under three-time instants (23, 25, and 27 years). In Fig. 6, the PDF during 23–27 years has two peaks; the "two-step translation method" can capture this feature with a smaller space step, Δf, and larger time step, Δt, than "approximate changing rate method". Thus, the "two-step translation method" is more suitable for deterioration with sudden damage. Fig. 7 compares the cumulative distribution function (CDF) between one million trails of MCS and the proposed PDFM, which demonstrates the accuracy and efficiency of the proposed method.

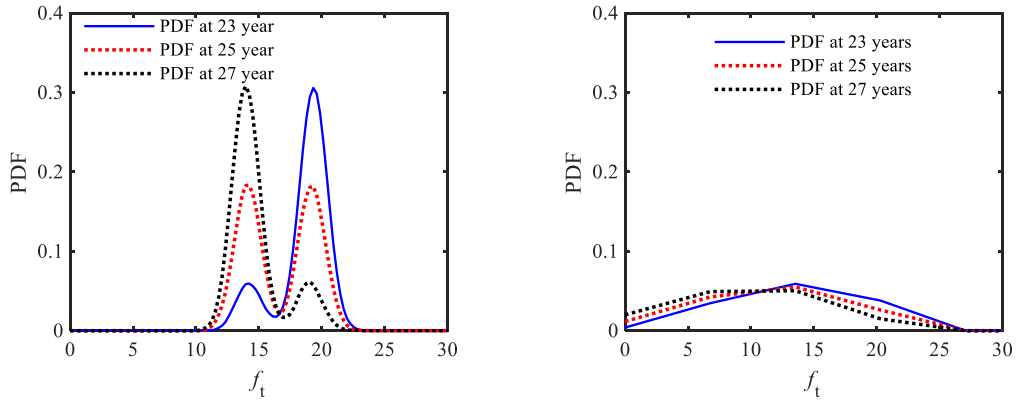

(a) "Two-step translation method" $\Delta t = 0.5$ year, $\Delta f = 0.268$

(b) "Approximate changing rate method" $\Delta t = 0.5$ year, $\Delta f = 7.748$

(c) "Approximate changing rate method" $\Delta t = 0.25$ year, $\Delta f = 1.937$

(d) "Approximate changing rate method" $\Delta t = 0.1$ year, $\Delta f = 0.290$

Fig. 6. Comparison of PDFs at 23, 25, and 27 years using different methods

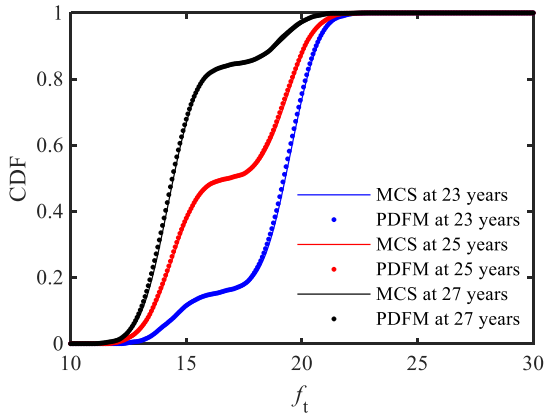

Fig. 7. CDFs at 23, 25, and 27 years using PDFM and MCS

Furthermore, considering multi-random and sudden events, a Poisson process $N(t)$ deteriorating system $f(t)$ is developed

$$f(t)=\left(1-6\times10^{-6}t^{3}\right)\cdot f_{0}-2\cdot\sum_{k=1}^{N(t)}H\left(t-t_{drop,k}\right),t_{drop,k}=\sum_{i=1}^{k}T_{i} \tag{32}$$

where, $t_{\mathrm{drop},k}$ is the time instant of k-th drop, and T_i is the i-th random variable following exponential distribution with λ of 0.04.

Considering repair after sudden events or threshold points, where performance would recover to the initial condition, the performance function $f(t)$ could be rewritten as

$$f(t)=\left(1-6\times10^{-6}t^{3}\right)\cdot f_{0}+H\left(t-t_{drop,k}\right)\cdot\left(6\times10^{-6}t^{3}\cdot f_{0}\right),t_{drop,k}=\sum_{i=1}^{k}T_{i} \tag{33}$$

According to Appendix A.1, 499 representative points were selected to achieve PDFM. Using the "two-step translation method", the PDF of $f(t)$, with and without repair actions, was calculated and is shown in Fig. 8, which is associated with an increased variation in time. Comparing Figs. 8c and d with Figs. 8a and b, essential maintenance could reduce the variation of the performance function.

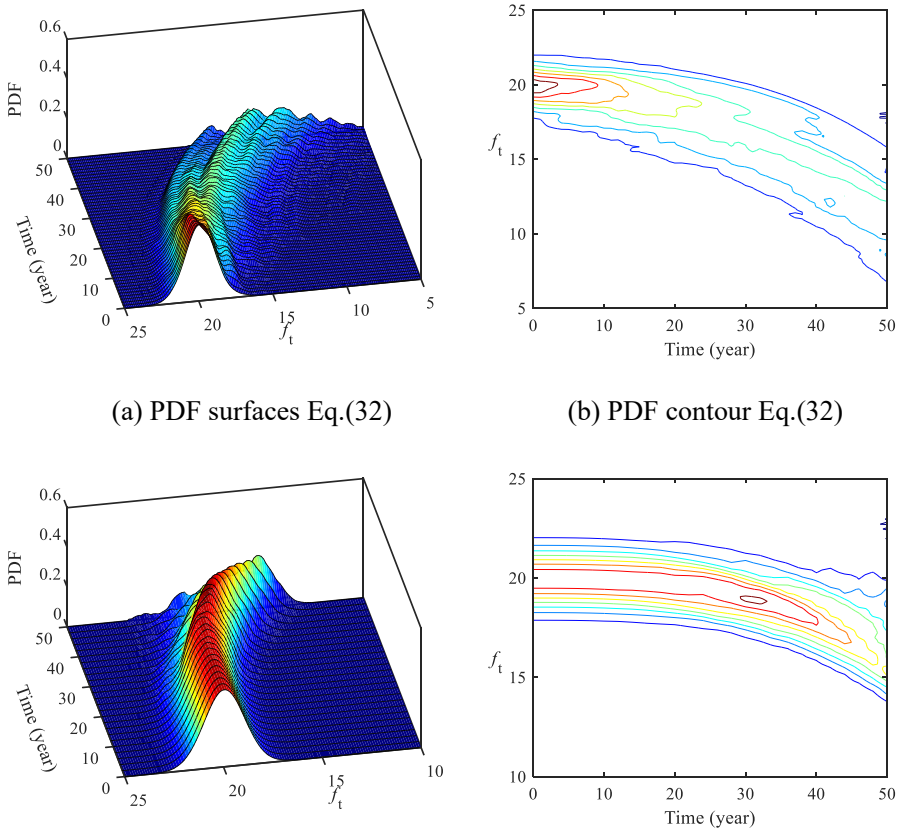

(a) PDF surfaces Eq.(32) (b) PDF contour Eq.(32)

(c) PDF surfaces Eq.(33) (d) PDF contour Eq.(33)

Fig. 8. PDF of a deteriorating system under multi-random sudden events

For the given three-time instants, Figs. 9a and 9c present the PDFs, and Figs. 9b and 9d present the CDFs, respectively. In Figs. 9a and 9c, the number of peaks increases with time, which is caused by the introduction of the Poisson process. Comparing Fig. 9c with 9a, when a repair action is applied at a given time instant, the mean of the performance function increases, but its standard deviation (STD) decreases. As indicated in Fig. 9sb and 9d, the curves of the CDF, computed by the PDFM, agree with those from MCS, which demonstrates that the proposed "two-step translation method" can be applied to a deteriorating system with multi-random sudden events. Furthermore, the effect of repair action on structural performance can be assessed using the proposed method.

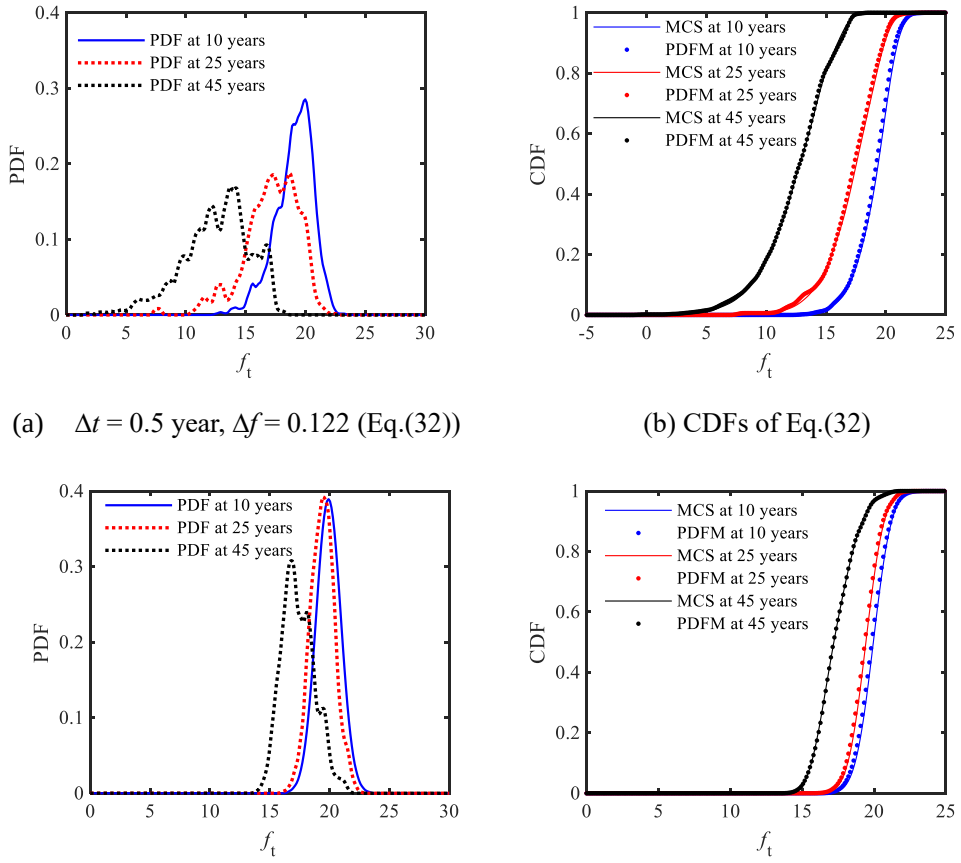

(a) $\Delta t = 0.5$ year, $\Delta f = 0.122$ (Eq.(32)) (b) CDFs of Eq.(32)

(c) $\Delta t = 0.5$ year, $\Delta f = 0.1214$ (Eq. (33)) (d) CDFs of Eq. (33)

Fig. 9. (a) PDFs and (b) CDF at 10, 25, and 45 years using the PDFM and MCS

3.2.Reliability analysis for one single section of an RC beam

In this section, a simply-supported beam with a cover of 25 mm was investigated. Its dimensions are 6000 mm × 200 mm × 500 mm. The beam was subjected to dead load G and live load Q. A single-row layout of reinforcement was designed: 4 ϕ 10 (A_s = 314 mm^2). The relevant distribution parameters of load, geometric, and material variables are summarized in Table 1. Considering the spatial variation of cross-sectional areas of corroded rebar, the beam was divided into m elements of length δ, as shown in Fig. 10.

In this case, length δ and m are denoted as 500 mm and 12, respectively, but only the mid-section of the RC beam is taken into consideration, and its performance function, $G_{mid}(\boldsymbol{\Theta}, t, \boldsymbol{b})$, is

$$G_{mid}(\boldsymbol{\Theta},t,\boldsymbol{b}) = M_{mid}(\boldsymbol{\Theta},t,\boldsymbol{b}) - S_{mid}(\boldsymbol{\Theta},t,\boldsymbol{b}) \tag{34}$$

where $M_{mid}(\boldsymbol{\Theta}, t, \boldsymbol{b})$ and $S_{mid}(\boldsymbol{\Theta}, t, \boldsymbol{b})$ are the flexural capacity and the load effect at time t, respectively.

Table 1 Variables of load, dimensions, and material

Variables	Distribution	Mean	Variation coefficient
Dead load G (kN/m)	Gaussian	$1.06G_k$	0.07
Durable live loads of residential buildings (kN/m^2)	Gumbel	$0.353Q_k$	0.23
Temporary live loads of residential buildings (kN/m^2)	Gumbel	$0.392Q_k$	0.32
f_c Compressive strength of concrete (MPa)	Gaussian	40	0.20
E_{st} Elastic modulus of the steel bar (MPa)	Gaussian	2×10^5	0.05
f_{y0} Yield strength of 10 mm diameter steel bar (MPa)	Gaussian	423	0.10
f_{y0} Yield strength of 14 mm diameter steel bar (MPa)	Gaussian	419	0.10
h_0 Effective depth of cross-section (mm)	Gaussian	480	0.02
b Width of cross-section (mm)	Gaussian	200	0.02

Note: G_k = 2.5 kN/m and Q_k = 2.0 kN/m^2.

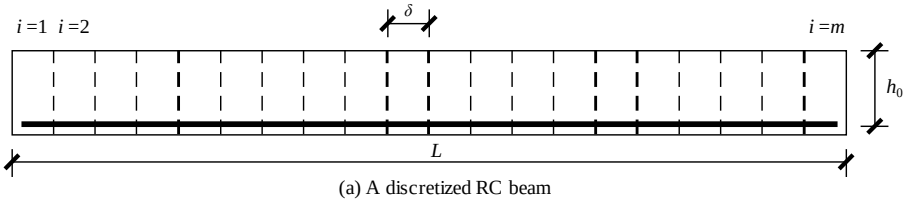

(a) A discretized RC beam

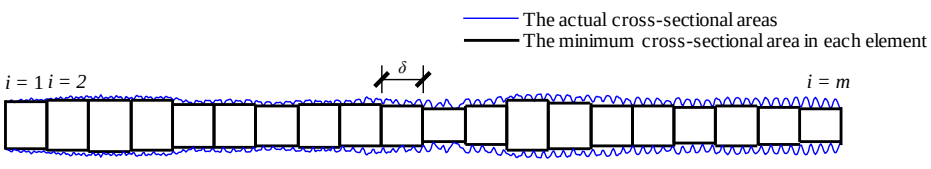

(b) The distribution of cross-sectional areas in a corroded rebar

Fig. 10. A discretized RC beam and cross-section of corroded rebar

3.2.1. *Differentiable deterioration model of an RC beam*

In this study, the mechanical performance of a corroded RC beam was evaluated using analytical models. With more information, the finite element method (FEM) could be used to assess structural performance. Given a well-anchored and completely bonded corroded RC beam, the flexural capacity of a corroded beam of the i-th element at time t, M_i (t) can be calculated as [45]

$$M_i(t) = F_{y,i}(t) \cdot \left[h_0 - \frac{F_{y,i}(t)}{2 f_c b} \right] \tag{35}$$

where $F_{y,i}$ (t) denotes the tensile capacity of corroded rebars of the i-th element at time t (N), f_c denotes concrete compressive strength (MPa), and b and h_0 denote the width and effective height (mm) of the beam section, respectively. The strength of the corroded rebar remains unchanged, and its tensile capacity is affected by the minimum cross-sectional area $A_{\min,j,i}$ (j =1,2,.., n and n is the number of tensile steel bars).

$$A_{\min,j,i} = \frac{A_{av}}{R} = \frac{\pi \left(D_0 - K \cdot i_{corr} \cdot t \right)^2}{4R} = \frac{\pi D_0^2 (1 - \eta_s)}{4R} \tag{36}$$

where A_{av} is the average residual cross-sectional area of the steel bar, D_0 denotes the initial diameter of the corroded steel bar, K is the Faraday constant at 0.0116 mm year^{-1}·(μA/cm^2)$^{-1}$, i_{corr} is the corrosion density of the steel bar, η_s denotes the average loss ratio of the cross-sectional area, and R is the corrosion non-uniformity factor following Gumbel distribution, whose parameters are denoted as μ and σ. In this case, i_{corr} is supposed as 2.3 μA/cm^2, and μ and σ are determined as follows [45]

$$\mu = 1.5544\eta_s + 1.01, \sigma = 0.3194\eta_s + 0.0006 \tag{37}$$

More detailed information about the calculation of corrosion ratio and factor R can be found in [45].

3.2.2. *Non-differentiable deterioration model of an RC beam*

Changing deterioration rate and sudden damage may happen within the service life of an RC beam due to the failure mechanisms of the tensile bar: brittle tensile failure and bond strength

loss. Fig. 11 compares the tensile capacity of steel bars under different failure modes, where bond strength loss may induce changing deterioration rates, and brittle tensile failure may cause sudden damage.

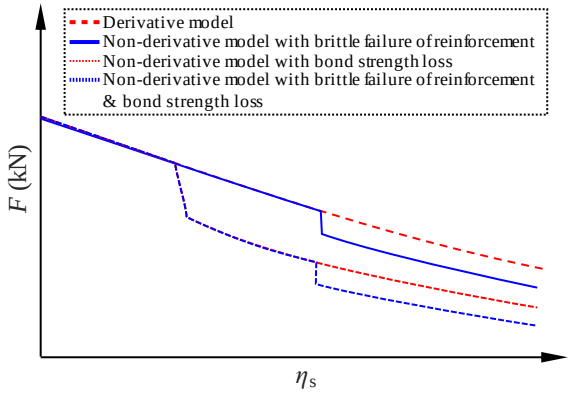

Fig. 11. Degradation curve of the tensile capacity of a steel bar under different failure modes

Existing studies have demonstrated that, with the development of corrosion, the mechanical performance of a corroded steel bar might change from ductile to brittle failure and its yield strain, strain hardening, and ultimate strength would also decrease. For instance, Cairns *et al*. [46] found that fracture strain declined to the yield strain under 20% corrosion degree, which is adopted by Stewart [30] as a critical corrosion degree. Zhang *et al.*'s [47] study found that the critical corrosion degree for the change of failure mode ranges from 20 to 30%. Gu *et al*. [45] found that the hardening and ultimate strain of corroded steel may not be as much with a higher corrosion degree and suggested using factor R as the critical factor of the change of failure mode. In terms of the previous mechanical test of the corroded rebar, when R reaches $[R]_{cr}$ = 1.3, the yield platform disappeared and brittle failure dominated. Accordingly, $F_{y,i}(t)$ could be calculated by [45]

$$F_{y,i}(t) = f_{y0} \cdot \max_{j=1}^{n}\left[i \cdot A_{\min,n+1-j,i}(t)\right] \cdot H\left(R-[R]_{cr}\right) + f_{y0} \cdot \left[\sum_{i=1}^{n} A_{\min,j,i}(t)\right] \cdot \left[1-H\left(R-[R]_{cr}\right)\right] \tag{38}$$

where, $A_{\min,i,j}(t)$ is the minimum cross-sectional area of the j-th rebar in the i-th element, which is ranked in an ascending order, i.e., $A_{\min,1,j}(t) < A_{\min,2,j}(t) < \cdots < A_{\min,n,j}(t)$.

On the other hand, Torres-Acosta *et al*. [48] found that the flexural capacity of an RC beam was dramatically reduced by bond strength loss under a corrosion ratio of 10%. Additionally,

Auyeung *et al.* [49] found that a 2% corrosion loss can lead to an 80% decline of bond strength. Thus, corrosion-induced loss of bond strength may significantly impair structural safety. In this case, the flexural strength of a corroded RC beam considering bond strength loss was computed by the model introduced in Appendix A.2.

3.2.3. *Reliability results of one single section*

Four failure modes were considered: the ductile tensile failure of the steel bar without bond strength loss (N ductile), the brittle tensile failure of the steel bar without bond strength loss (N brittle), the ductile failure of the steel bar with bond strength loss (Y ductile), and the brittle failure of the steel bar without bond strength loss (Y brittle). There were 12 random variables, including four factor-R and eight variables of load, dimensions, and material. Based on the proposed algorithm of PDFM in section 2 and point set strategies in appendix A.1, 599 representative points were selected to solve GDEE and the residual PDF, $p^*_G(g, t)$, was evaluated under different failure modes. Figs. 12 and 13 show the PDF surfaces at given time intervals and the contour plot of $p^*_G(g, t)$, which do not contain the negative part due to the absorbing boundary condition. The PDF surface in Fig. 12a and contour in Fig. 13a were much smoother than Figs. 12b, c, d, and Figs. 13b, c, d, respectively. Comparing Fig. 12a with Fig.12b, $p^*_G(g, t)$ became rough from the 22nd to the 32nd year, considering the brittle tensile failure of the steel bar. Then, $p^*_G(g, t)$ became more rugged from the 14th to the 24th year after considering bond strength loss. Furthermore, comparing Fig. 13c with 13d, the ruggedness of $p^*_G(g, t)$ did not increase considering both the brittle failure of the corroded steel bar and bond strength loss.

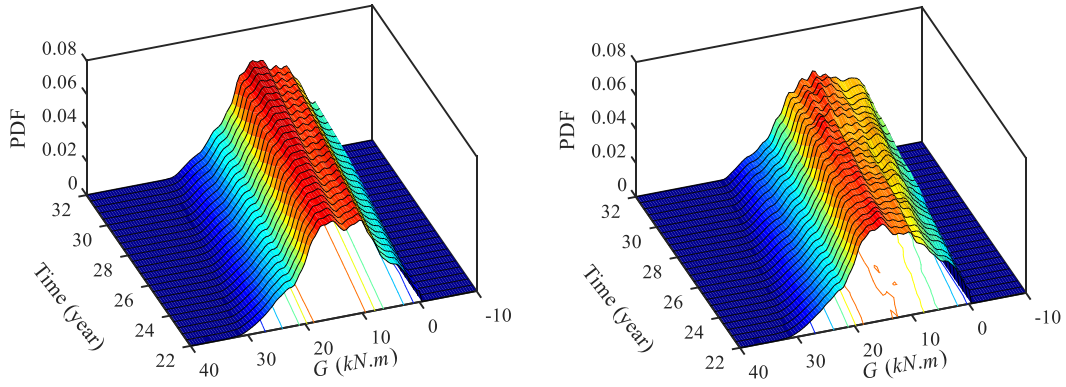

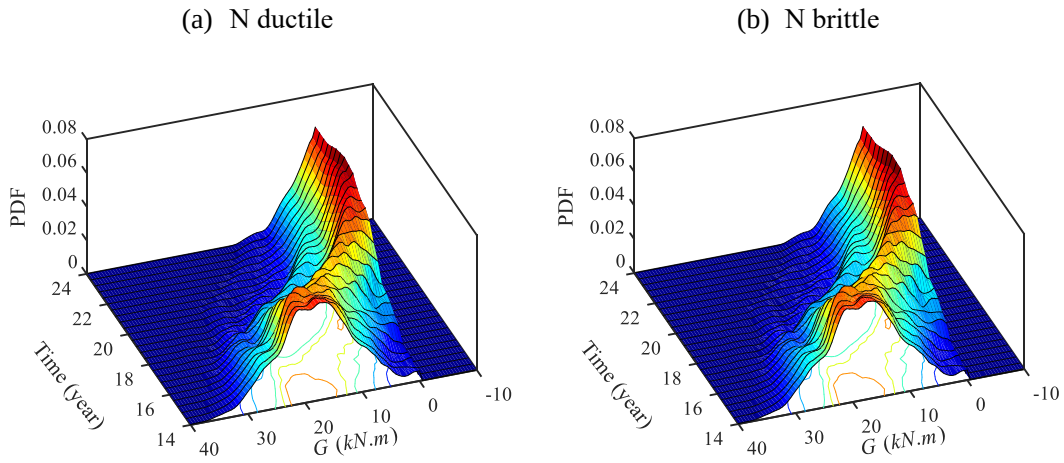

(a) N ductile (b) N brittle

(c) Y ductile (d) Y brittle

Fig. 12. PDF surface of four failure modes at typical time intervals

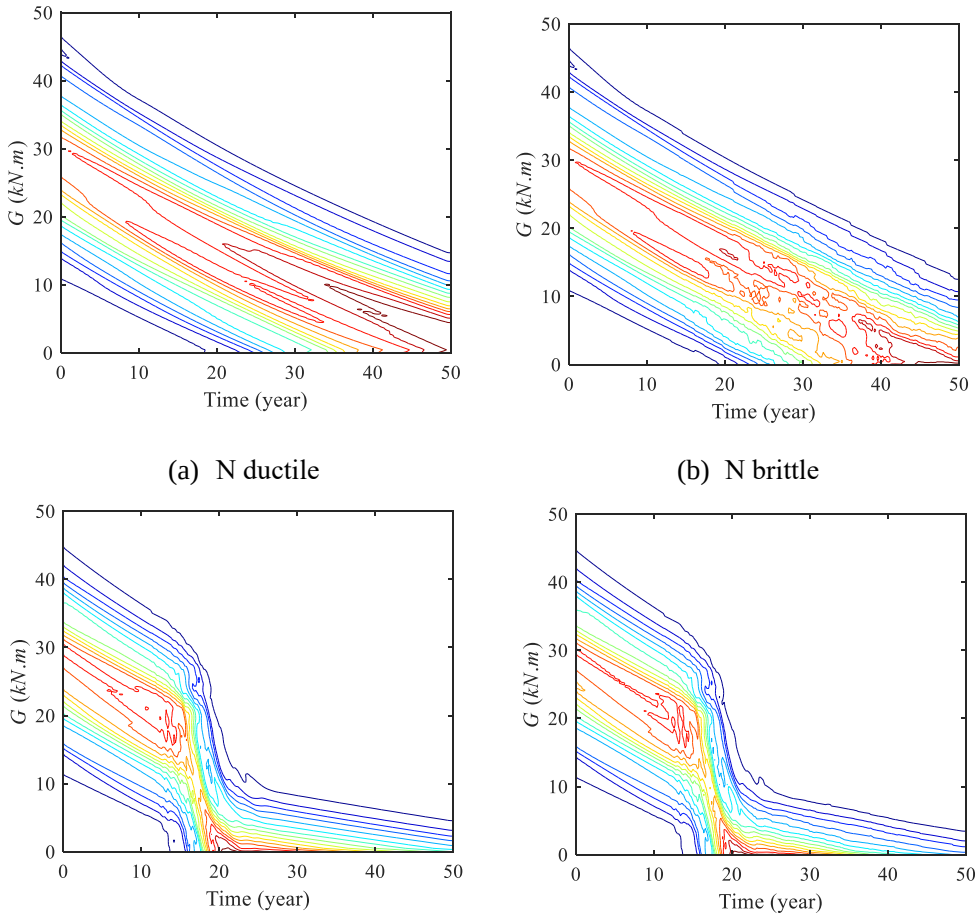

(a) N ductile (b) N brittle

(c) Y ductile (d) Y brittle

Fig. 13. PDF contour plot of four failure modes

Fig. 14 compares the mean and standard deviation (STD) of $G(\boldsymbol{\Theta},t,\mathbf{b})$ calculated by the proposed method, $\mu_{PDFM,}$ and σ_{PDFM}, with those of 1,000,000 trials of MCS, $\mu_{MCS,}$ and σ_{MCS}. In Fig. 14, the μ_{PDFM} and σ_{PDFM} agree with μ_{MCS} and σ_{MCS}. The relative errors of μ_{PDFM} and σ_{PDFM},

viz. $e_{\|\mu\|}$ and $e_{\|\sigma\|}$, can be calculated by the ratio of $\left\|\mu_{PDET}(t)-\mu_{MCS}(t)\right\|_2$ to $\left\|\mu_{MCS}(t)\right\|_2$ and the ratio of $\left\|\sigma_{PDET}(t)-\sigma_{MCS}(t)\right\|_2$ to $\left\|\sigma_{MCS}(t)\right\|_2$, respectively. Results of $e_{\|\mu\|}$ and $e_{\|\sigma\|}$ are listed in Table 2 where $e_{\|\mu\|}$ varies from 1.232% to 2.903% and $e_{\|\sigma\|}$ varies from 1.101% to 1.883%. The consumed time is 13 s using the PDFM but 112 s with MCS. Such a comparison of results verifies the feasibility and efficiency of the proposed approach in time-dependent reliability analysis.

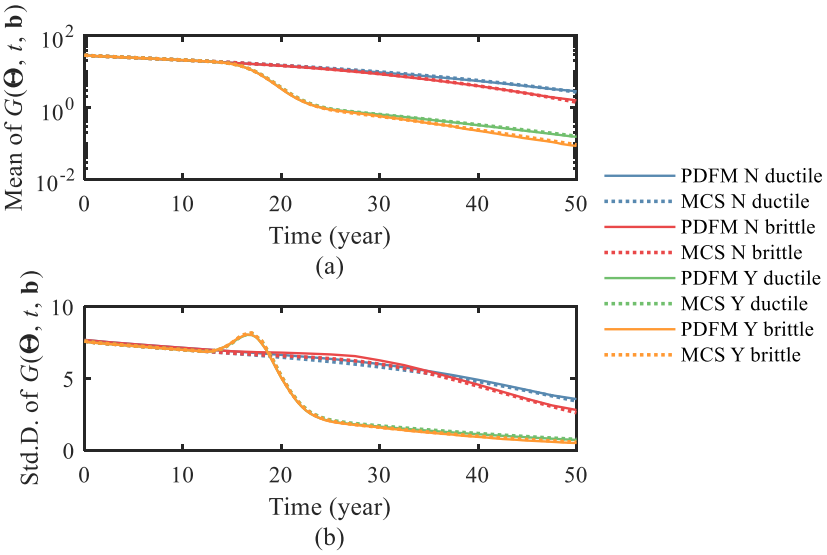

Fig. 14. Mean and STD of $G(\boldsymbol{\Theta}, t, \mathbf{b})$ using the PDFM and MCS

Table 2. Relative errors of μ_{PDFM} and σ_{PDFM}

Failure mode	N ductile	N brittle	Y ductile	Y brittle
μ_{PDFM}	2.372%	2.903%	1.314%	1.232%
σ_{PDFM}	1.883%	1.867%	1.101%	1.103%

Fig. 14a shows that the μ_{PDFM} of Y ductile and Y brittle declines rapidly in the 14th year, while the μ_{PDFM} of N ductile and N brittle look much slower. However, in Fig. 14b, the σ_{PDFM} of Y ductile and Y brittle rises 19% from the 13th to the 17th year and then dropps rapidly. Thus, considering bond strength loss may increase the uncertainty of the service life of a corroded RC beam.

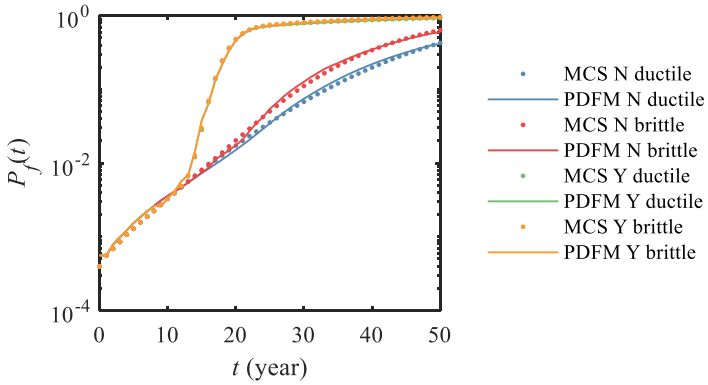

Fig. 15. Time-dependent $p_f(t)$ under different failure modes

The failure probability, $p_f(t)$, can be calculated by Eq.(6). For simplified consideration, the $p_f(t)$ of N ductile is denoted as $p_{f1}(t)$, the $p_f(t)$ of N brittle is $p_{f2}(t)$, the $p_f(t)$ of Y ductile is $p_{f3}(t)$, and the $p_f(t)$ of Y brittle is $p_{f4}(t)$. Fig. 15 presents the $p_f(t)$ calculated by the proposed method and MCS of 1,000,000 trials (F_{MCS}), where F_{PDFM} agrees with F_{MCS}.

3.3.Reliability analysis for a series system study of an RC beam

Due to the influence of the uncertain and random properties of environmental parameters, the failure location of the RC beam might not be at the point of maximum load effect [5,21,50]. The length, δ, is also denoted as 500 mm, the performance function of the whole beam, $G(\boldsymbol{\Theta}, t, \boldsymbol{b})$, refers to Eq.(2), and the performance function of the i-th element, $G_i(\boldsymbol{\Theta}, t, \boldsymbol{b})$, could be expressed as

$$G_i(\boldsymbol{\Theta},t,\boldsymbol{b}) = M_i(\boldsymbol{\Theta},t,\boldsymbol{b}) - S_i(\boldsymbol{\Theta},t,\boldsymbol{b}) \tag{39}$$

where $\boldsymbol{\Theta} = [\theta_1, \theta_2, \ldots, \theta_d]^T$ is the random vector with d-elements representing all related variables, and $M_i(\boldsymbol{\Theta}, t, \boldsymbol{b})$ and $S_i(\boldsymbol{\Theta}, t, \boldsymbol{b})$ are the flexural capacity and the load effect of the i-th element at time t, respectively. Moreover, due to non-uniform corrosion-induced spatial effects, M_i varies in each segment. Thus, $G(\boldsymbol{\Theta}, t, \boldsymbol{b})$ may be non-differentiable several times, and its progressive derivative is dramatic and towards minus infinity in several instantaneous time instants, as illustrated in Fig. 1.

Two single-row layouts of reinforcement were designed: 4 ϕ 10 (A_s = 314 mm^2) and 2 ϕ 14 (A_s = 307.8 mm^2). The distribution parameters of factor R are listed in Table 3. Six numerical

cases were made to study the influences of failure mode, corrosion rate, and steel bar diameter on the reliability of the corroded RC beam. All R factors were assumed to be independent variables based on the autocorrelation function (ACF) analysis of cross-sectional areas. For more detailed information, refer to [45].

For cases 1–5, there were 56 random variables, including 48 factor R and eight variables of load, dimensions, and material. For case 6, there were 32 random variables, including 24 factor R and eight variables of load, dimensions, and material. Additionally, due to the involvement of more random variables, 700 representative points were selected through the method in Appendix A.1 to conduct the PDFM. Case 1 was then taken as an example to verify the feasibility and efficiency of the proposed PDFM in finding the solution to PDF. For case 1, PDFM and MCS take about 48 s and 1116 s, respectively.

Table 3 Distribution parameters of corrosion non-uniformity factor under the δ of 500 mm

Case	D_0 (mm)	i_{corr} (μA/cm^2)	Gumbel distribution parameters	
			μ	σ
1	10	2.3	1.5544η_s+1.01	0.3194η_s+0.0006
2	10	4.5	1.4436η_s+1.01	0.3194η_s+0.0006
3	10	9.1	1.2214η_s+1.01	0.3194η_s+0.0006
4	10	13	1.1η_s+1.01	0.3527η_s+0.0006
5	10	19	0.9673η_s+1.01	0.3527η_s+0.0006
6	14	19	0.6235η_s+1.013	0.2508η_s+0.0011

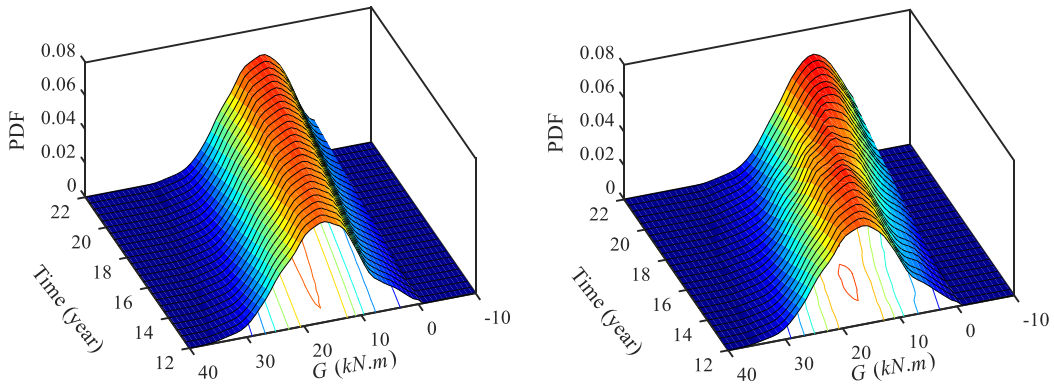

(a) N ductile (b) N brittle

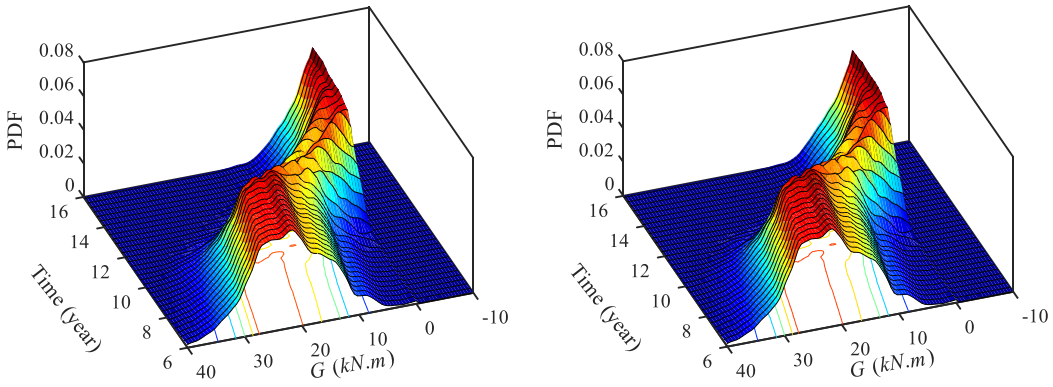

(c) Y ductile (d) Y brittle

Fig. 16. PDF surfaces of case 1 at given time intervals under different failure modes

Figs. 16 and 17 show the PDF surfaces, $p^*_G(g, t)$, of case 1, which do not contain the negative part due to the absorbing boundary condition. PDF surfaces and contours in Figs. 16a and 17a are much smoother than those in Figs. 16b, c, d, and Figs. 17b, c, d. Comparing Figs. 16a and 17a with Figs. 16b and 17b, PDF surfaces became rough from the 12th to the 22nd year, considering the brittle tensile failure of the corroded steel bar. Additionally, PDF surfaces became more rugged from the 6th to the 16th year after considering bond strength loss. Similarly, comparing Figs. 16c and 17c with Figs. 16d and 17d, the ruggedness of PDF surfaces does not change apparently.

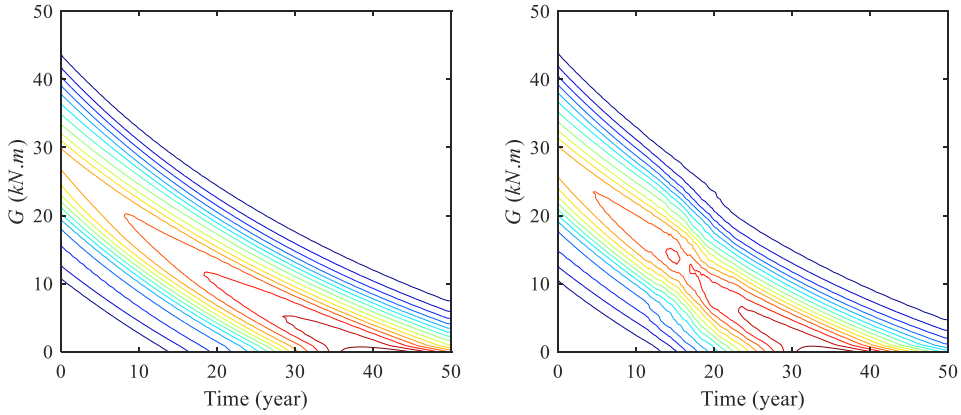

(a) N ductile (b) N brittle

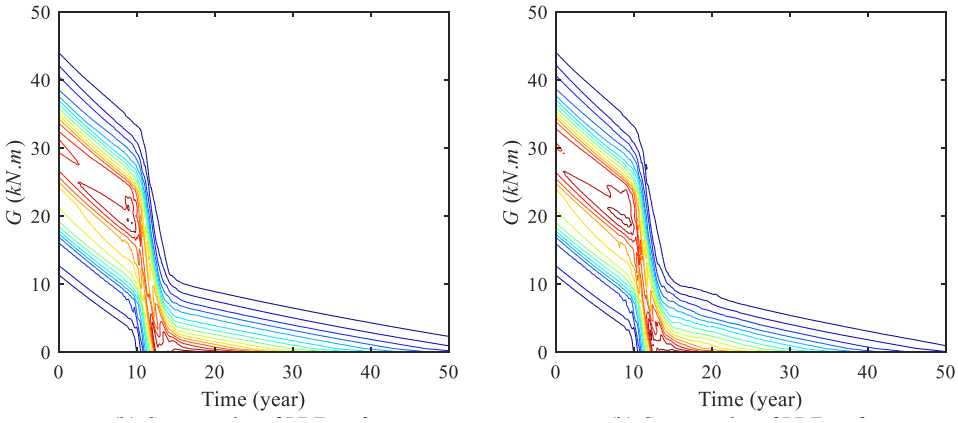

(d) Y ductile (d) Y brittle

567 Fig. 17. PDF contour plot of case 1 at given time intervals under different failure modes

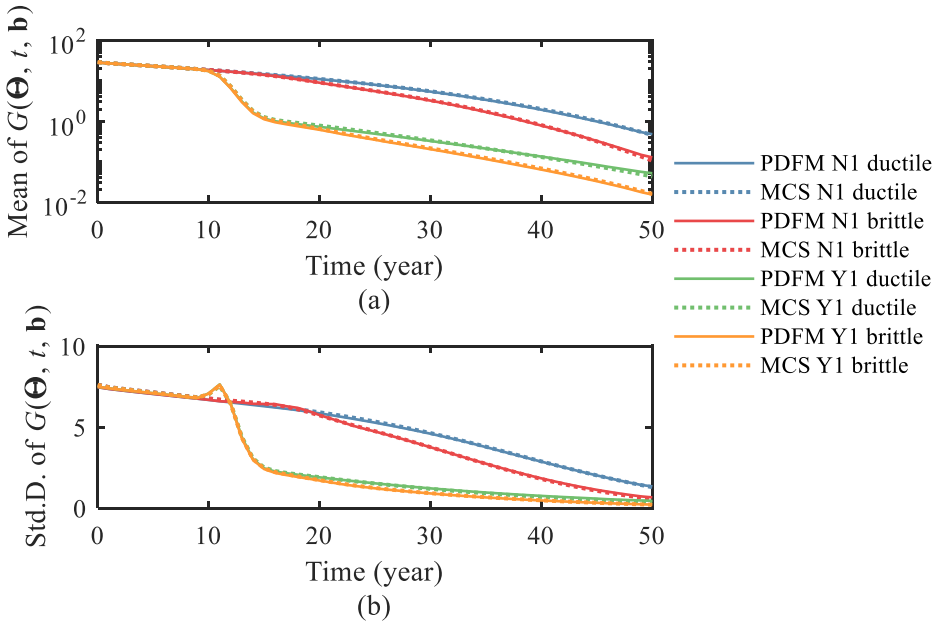

568
569 Fig. 18. (a) Mean and (b) STD of $G(\boldsymbol{\Theta}, t, \boldsymbol{b})$ using the PDFM and MCS in case 1
570

571 Fig. 18 also compares $\mu_{PDFM,}$ and σ_{PDFM} with $\mu_{MCS,}$ and σ_{MCS}, and the results of $e_{\|\mu\|}$ and $e_{\|\sigma\|}$
572 are listed in Table 4, where $e_{\|\mu\|}$ varies from 0.917% to 1.941% and $e_{\|\sigma\|}$ varies from 0.826% to
573 1.272%. Fig. 18a also shows that the μ_{PDFM} of Y ductile and Y brittle declines rapidly in the
574 ninth year, while the μ_{PDFM} of N ductile and N brittle look much slower. However, in Fig. 18b,
575 the σ_{PDFM} of Y ductile and Y brittle rises 11% from ninth to the 11th year and then dropps rapidly.
576 Thus, considering bond strength loss may increase the uncertainty in the service life of the
577 corroded RC beam.

578 Table 4 Relative error of μ_{PDFM} and σ_{PDFM} under case 1

Failure mode	N ductile	N brittle	Y ductile	Y brittle

μ_{PDFM}	0.984%	0.917%	1.941%	1.912%
σ_{PDFM}	1.257%	1.263%	1.272%	0.826%

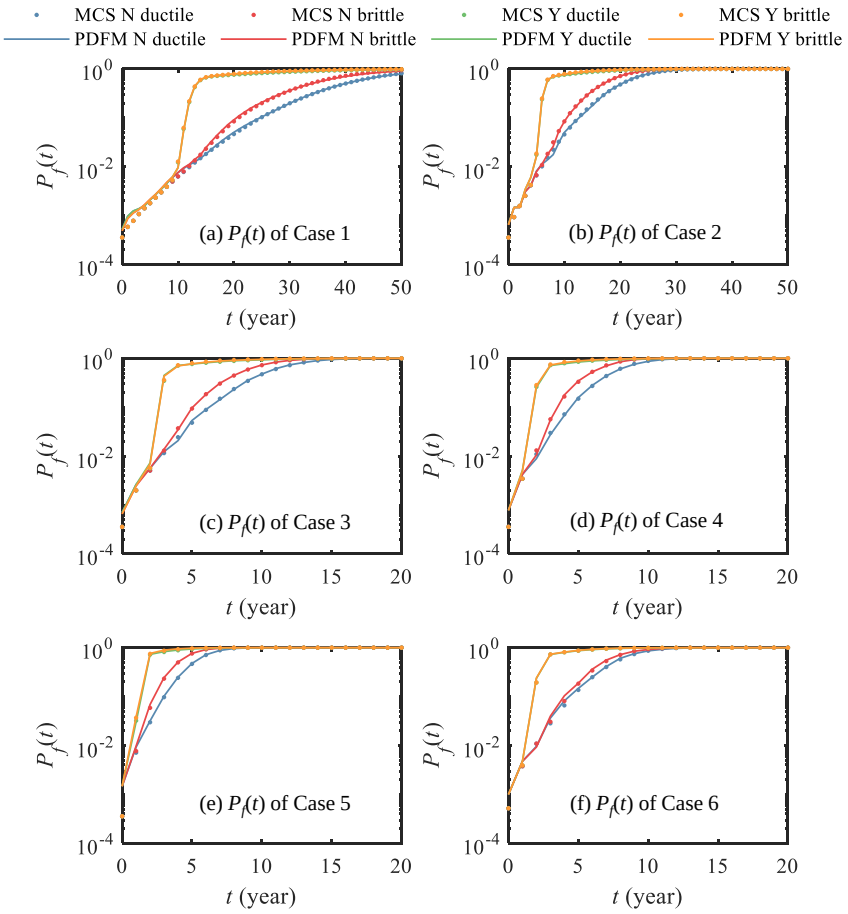

Fig. 19. Calculation results of $p_f(t)$ in all cases

Fig. 19 presents the $p_f(t)$ and $\beta(t)$ of all numerical cases under different failure modes and were calculated by the proposed method and MCS of 1,000,000 trials (F_{MCS}), where F_{PDFM} agrees with F_{MCS} in all cases. Estimated results are summarized in Table 5, which shows the relative errors in the $p_f(t)$ range from 0.29% to 2.71%. Thus, in system-level cases, the proposed method has high efficiency and precision in reliability calculation.

Table 5 Relative errors of $p_f(t)$ for all cases

Case	$p_{f1}(t)$	$p_{f2}(t)$	$p_{f3}(t)$	$p_{f4}(t)$
1	1.08%	2.71%	0.53%	0.68%
2	0.75%	0.40%	0.58%	0.46%
3	0.44%	0.29%	1.50%	1.44%
4	0.55%	0.47%	0.44%	0.62%
5	0.36%	0.38%	0.40%	0.55%

6	0.82%	0.86%	0.71%	0.78%

3.3.1. Influences of failure mode

Fig. 19 shows that failure mode has an apparent effect on $p_f(t)$. For $p_f(t)$ in Fig. 19, $p_{f4}(t)$ has the fastest varying rate, followed by $p_{f3}(t)$, $p_{f2}(t)$, and $p_{f1}(t)$. Thus, bond strength loss has more influence on the reliability of the corroded RC beam than the brittle failure of the corroded steel bar. All curves of Y ductile and Y brittle in Fig. 19 are associated with a three-stage process: $p_f(t)$ increases slowly as N ductile and N brittle, $p_f(t)$ increases rapidly, and $p_f(t)$ increases gradually, in which the differences between $p_{f3}(t)$ and $p_{f4}(t)$ appear mainly in the third stage. Furthermore, all curves with N brittle experience a two-stage process: $p_f(t)$ increases as slowly as $p_{f1}(t)$, and $p_f(t)$ grows faster than $p_{f1}(t)$. The critical time instants of the velocity change of $p_f(t)$ are listed in Table 6.

Table 6. Critical time instants of $p_f(t)$ evolution

Case		1	2	3	4	5	6
Y ductile	1st point (year)	9	4	2	1	0	1
&Y brittle	2nd point (year)	15	8	4	3	2	3
N brittle		12	6	3	2	1	3

Comparing the values of p_f with different η_s and i_{corr} in Table 7, $p_{f2}(t)$ is 1.16–2.22 times $p_{f1}(t)$, $p_{f3}(t)$ is 1.20–35.43 times $p_{f1}(t)$, $p_{f4}(t)$ is 1.22–36.07 times $p_{f1}(t)$, and $p_{f4}(t)$ is 1.01–1.07 times $p_{f4}(t)$. The differences among $p_{f1}(t)$, $p_{f2}(t)$, $p_{f3}(t)$, and $p_{f4}(t)$ decrease with the increase of η_s. Thus, considering bond strength loss may dramatically increase failure probability and diminish the effect brought by the brittle failure of the steel bar.

Table 7. p_f under different η_s and i_{corr}

η_s	i_{corr} (μA/cm^2)	Failure probability				The ratio of failure probability			
		p_{f1}	p_{f2}	p_{f3}	p_{f4}	p_{f2}/p_{f1}	p_{f3}/p_{f1}	p_{f4}/p_{f1}	p_{f4}/p_{f3}
0.1	2.3	0.020	0.026	0.681	0.691	1.32	34.59	35.11	1.02
	4.6	0.018	0.023	0.631	0.643	1.30	35.43	36.07	1.02
	9.1	0.015	0.019	0.431	0.445	1.28	29.56	30.55	1.03
	13.0	0.013	0.019	0.323	0.346	1.41	23.95	25.69	1.07
	19.0	0.013	0.022	0.221	0.232	1.62	16.53	17.35	1.05
0.2	2.3	0.257	0.447	0.890	0.926	1.74	3.46	3.60	1.04
	4.6	0.228	0.414	0.881	0.919	1.81	3.86	4.02	1.04
	9.1	0.179	0.351	0.861	0.904	1.97	4.82	5.07	1.05

	13.0	0.158	0.345	0.851	0.902	2.18	5.38	5.69	1.06
	19.0	0.141	0.314	0.836	0.886	2.22	5.93	6.29	1.06
	2.3	0.812	0.941	0.975	0.989	1.16	1.20	1.22	1.01
	4.6	0.781	0.929	0.972	0.987	1.19	1.25	1.27	1.02
0.3	9.1	0.688	0.886	0.962	0.982	1.29	1.40	1.43	1.02
	13.0	0.644	0.877	0.956	0.981	1.36	1.48	1.52	1.03
	19.0	0.578	0.835	0.947	0.976	1.44	1.64	1.69	1.03

606

607 *3.3.2. Influences of corrosion rate*

608 Fig. 20 compares p_{f2} and p_{f4} under different i_{corr}. In Fig. 20a, the increasing rates of $p_{f2}(t)$ and
609 $p_{f4}(t)$ versus t both increase with a rising corrosion rate. However, in Fig. 20b, the increasing
610 rates of $p_{f2}(t)$ and $p_{f4}(t)$ versus η_s decrease with a rising corrosion rate, except for "p_{f4} of 19.0
611 μA/cm^2" initially because 19.0 μA/cm^2 causes about 8% of η_s within the first year. In other
612 words, under a given corrosion degree and the consideration of corrosion non-uniformity, the
613 smaller the corrosion rate, the less safe the corroded beam is.

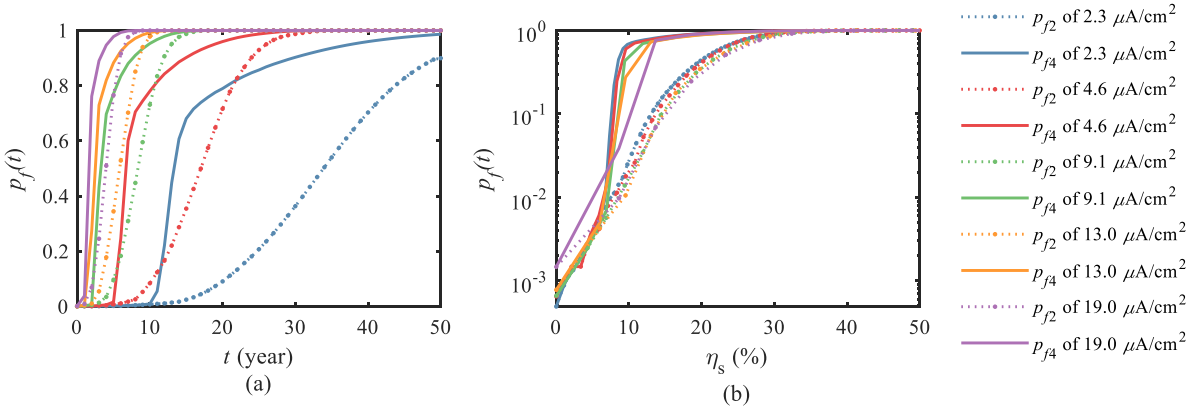

614

615 Fig. 20. (a) $p_{f2}(t)$ and (b) $p_{f4}(t)$ under different i_{corr}

616 *3.3.3. Influences of rebar diameters*

617 Fig. 21 shows $p_{f2}(t)$ and $p_{f4}(t)$ with different rebar diameters D_{s0} (10 mm or 14 mm) and the
618 same corrosion rate (i_{corr} = 19 μA/cm^2). This figure illustrates that $p_{f2}(t)$ and $p_{f4}(t)$ with small
619 D_{s0} are higher than those with a larger D_{s0} because the slopes of μ and σ versus η_s of the 10 mm
620 diameter rebar are both larger than those of the 14 mm diameter rebar. However, considering
621 bond strength loss, the influences of rebar diameter on $p_{f4}(t)$ seem to be diminished during the
622 first three years (η_s ranges about 0–0.15). Hence, the $p_f(t)$ of the 10 mm diameter rebar may be

higher than that of the 14 mm diameter rebar. Although such an effect may not be so apparent with the consideration of bond strength loss, larger diameter rebar can increase the reliability and safety of a corroded RC beam [45].

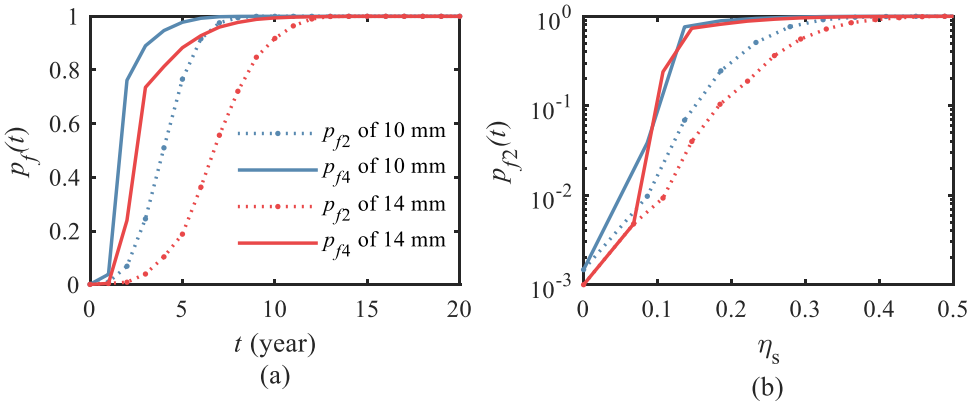

Fig. 21. (a) $p_{f2}(t)$ and (b) $p_{f4}(t)$ under different diameters

4. Conclusions

This paper proposed a general framework for time-dependent reliability analysis of deteriorating structures in a life-cycle context. A novel PDFM approach was developed to compute the time-dependent reliability under different deterioration processes: continuous deterioration and sudden events. Then, three application examples were made to assess the feasibility and efficiency of the proposed framework; the following conclusions were obtained:

(1) For Type I continuous deterioration (i.e., differentiable performance function), classical PDFM could be applied to obtain PDF and reliability directly. For the deterioration system with discontinuous derivative function, the "approximate changing rate method" could be used. However, for the deterioration system with sudden events, the "approximate changing rate method" not be appropriate to obtain satisfying analysis results, which was verified in the first application example. To solve this issue, the "two-step translation method" was developed, which was theoretically approved and numerically verified by the three application examples.

(2) In reliability analysis of a single section at the corroded RC beam, the deviations of mean and STD for performance function were about 1.1%–2.9%, and the relative errors of failure probability were quite small comparing the PDFM with 1,000,000 trials of MCS.

(3) For reliability analysis at system level, the deviations of mean and STD for performance function were about 0.9%–1.9%, and the relative errors of failure probability were about 0.29%–2.71%, comparing PDFM with 1,000,000 samples of MCS. A relatively low point selection and relative error prove the efficiency and accuracy of the proposed method. Sensitivity analysis shows that failure mode has an essential effect on reliability calculation, especially in the degree of low corrosion. With the consideration of bond strength loss, failure probability may increase about 34 times; considering the brittle failure of the steel bar, failure probability may increase by 120%. Furthermore, whether considering bond strength loss or not, a lower corrosion rate may cause lower reliability under a given corrosion level. On the other hand, a steel bar with a large diameter may have higher reliability, but such an effect was limited once bond strength loss was considered.

In summary, it is feasible, robust, and efficient to apply the proposed framework to conduct time-dependent reliability analysis of deteriorating structures under different deterioration mechanisms and scenarios. The proposed framework overcomes the demerits of previous PDFM and enriches the toolbox to aid life-cycle design and maintenance. The analytical models were employed in this paper for the development of the performance function. In the future, more studies are needed to adopt the FEM technology and to take the effect of hazard events on progressive deterioration, etc. into consideration. The proposed method could also be extended to a larger scale application in other engineering fields. Additionally, illustrative examples showed that the proposed method could be implemented in high-dimensional scenarios (e.g. 56 random input variables). In the future, it would also be beneficial to apply the proposed method to higher-dimensional situations and to enhance the robustness of the proposed method.

5. Acknowledgments

Funding: The authors gratefully acknowledge the financial support of the National Natural Science Foundation of China (Grant No. 51320105013 and Grant No. 51808476), the National Basic Research Program of China (973 program) (Grant No. 2015CB655100), and Research

673 Grants Council of the Hong Kong Special Administrative Region, China (Grant No. PolyU
674 252161/18E).

675 **6. References:**

676 [1] Frangopol DM, Dong Y, Sabatino S. Bridge life-cycle performance and cost: analysis,
677 prediction, optimisation and decision-making. Struct Infrastruct Eng 2017;13:1239–57.
678 https://doi.org/10.1080/15732479.2016.1267772.
679 [2] Akiyama M, Frangopol DM, Ishibashi H. Toward life-cycle reliability-, risk- and
680 resilience-based design and assessment of bridges and bridge networks under
681 independent and interacting hazards: emphasis on earthquake, tsunami and corrosion.
682 Struct Infrastruct Eng 2019;0:1–25. https://doi.org/10.1080/15732479.2019.1604770.
683 [3] Mori Y, Ellingwood BR. Reliability-based service-life assessment of aging concrete
684 structures. J Struct Eng (United States) 1993;119:1600–21.
685 https://doi.org/10.1061/(ASCE)0733-9445(1993)119:5(1600).
686 [4] Frangopol DM, Lin K, Estes AC. Reliability of Reinforced Concrete Girders under
687 Corrosion Attack. J Struct Eng 1997;123:286–97. https://doi.org/10.1061/(ASCE)0733-
688 9445(1997)123:3(286).
689 [5] Stewart MG. Spatial variability of pitting corrosion and its influence on structural
690 fragility and reliability of RC beams in flexure. Struct Saf 2004;26:453–70.
691 https://doi.org/10.1016/j.strusafe.2004.03.002.
692 [6] Wang L, Dai L, Bian H, Ma Y, Zhang J. Concrete cracking prediction under combined
693 prestress and strand corrosion. Struct Infrastruct Eng 2019;15:285–95.
694 https://doi.org/10.1080/15732479.2018.1550519.
695 [7] Guo HY, Dong Y, Gu XL. Durability assessment of reinforced concrete structures
696 considering global warming: A performance-based engineering and experimental
697 approach. Constr Build Mater 2020;233:117251.
698 https://doi.org/10.1016/j.conbuildmat.2019.117251.
699 [8] Tu B, Fang Z, Dong Y, Frangopol DM. Time-variant reliability analysis of widened
700 deteriorating prestressed concrete bridges considering shrinkage and creep. Eng Struct

2017;153:1–16. https://doi.org/10.1016/j.engstruct.2017.09.060.

[9] Tu B, Dong Y, Fang Z. Time-Dependent Reliability and Redundancy of Corroded Prestressed Concrete Bridges at Material, Component, and System Levels. J Bridg Eng 2019;24. https://doi.org/10.1061/(ASCE)BE.1943-5592.0001461.

[10] Wang Z, Jin W, Dong Y, Frangopol DM. Hierarchical life-cycle design of reinforced concrete structures incorporating durability, economic efficiency and green objectives. Eng Struct 2018;157:119–31. https://doi.org/10.1016/j.engstruct.2017.11.022.

[11] Wang C, Zhang H, Li Q. Reliability assessment of aging structures subjected to gradual and shock deteriorations. Reliab Eng Syst Saf 2017;161:78–86. https://doi.org/10.1016/j.ress.2017.01.014.

[12] Sanchez-Silva M, Klutke GA, Rosowsky D V. Life-cycle performance of structures subject to multiple deterioration mechanisms. Struct Saf 2011;33:206–17. https://doi.org/10.1016/j.strusafe.2011.03.003.

[13] Kumar R, Cline DBH, Gardoni P. A stochastic framework to model deterioration in engineering systems. Struct Saf 2015;53:36–43. https://doi.org/10.1016/j.strusafe.2014.12.001.

[14] Li Y, Dong Y, Frangopol DM, Gautam D. Long-term resilience and loss assessment of highway bridges under multiple natural hazards. Struct Infrastruct Eng 2020;16:626–41. https://doi.org/10.1080/15732479.2019.1699936.

[15] Frangopol DM. Reliability Deterioration and Lifetime Maintenance Cost Optimization. Keynote Lect Proc First Int ASRANet Colloq Integr Struct Reliab Anal with Adv Struct Anal 2002:1–14.

[16] Van Noortwijk JM, Frangopol DM. Two probabilistic life-cycle maintenance models for deteriorating civil infrastructures. Probabilistic Eng Mech 2004;19:345–59. https://doi.org/10.1016/j.probengmech.2004.03.002.

[17] Frangopol DM, Das PC. Management of bridge stocks based on future reliability and maintenance costs. Bridg Des Constr Maint 1999:45–58.

[18] Kamiński M. The Stochastic Perturbation Method for Computational Mechanics. 2013.

https://doi.org/10.1002/9781118481844.

[19] Li CQ. Life-cycle modeling of corrosion-affected concrete structures: Propagation. J Struct Eng 2003;129:753–61. https://doi.org/10.1061/(ASCE)0733-9445(2003)129:6(753).

[20] Li CQ, Melchers RE. Time-dependent risk assessment of structural deterioration caused by reinforcement corrosion. ACI Struct J 2005;102:754–62. https://doi.org/10.14359/14671.

[21] Stewart MG, Al-Harthy A. Pitting corrosion and structural reliability of corroding RC structures: Experimental data and probabilistic analysis. Reliab Eng Syst Saf 2008;93:373–82. https://doi.org/10.1016/j.ress.2006.12.013.

[22] El Hassan J, Bressolette P, Chateauneuf A, El Tawil K. Reliability-based assessment of the effect of climatic conditions on the corrosion of RC structures subject to chloride ingress. Eng Struct 2010;32:3279–87. https://doi.org/10.1016/j.engstruct.2010.07.001.

[23] Zhang M, Song H, Lim S, Akiyama M, Frangopol DM. Reliability estimation of corroded RC structures based on spatial variability using experimental evidence, probabilistic analysis and finite element method. Eng Struct 2019;192:30–52. https://doi.org/10.1016/j.engstruct.2019.04.085.

[24] Li CQ. Computation of the failure probability of deteriorating structural systems. Comput Struct 1995;56:1073–9. https://doi.org/10.1016/0045-7949(94)00947-2.

[25] Bastidas-Arteaga E, Bressolette P, Chateauneuf A, Sánchez-Silva M. Probabilistic lifetime assessment of RC structures under coupled corrosion-fatigue deterioration processes. Struct Saf 2009;31:84–96. https://doi.org/10.1016/j.strusafe.2008.04.001.

[26] Tran TV, Bastidas-Arteaga E, Schoefs F, Bonnet S, O'Connor AJ, Lanata F. Structural reliability analysis of deteriorating RC bridges considering spatial variability. Bridg Maintenance, Safety, Manag Resil Sustain - Proc Sixth Int Conf Bridg Maintenance, Saf Manag 2012:698–705. https://doi.org/10.1201/b12352-94.

[27] Ciampoli M, Ellingwood B. Probabilistic methods for assessing current and future performance of concrete structures in nuclear power plants. Mater Struct 2002;35:3–14.

[28] Yang DY, Frangopol DM. Life-cycle management of deteriorating civil infrastructure considering resilience to lifetime hazards: A general approach based on renewal-reward processes. Reliab Eng Syst Saf 2019;183:197–212. https://doi.org/10.1016/j.ress.2018.11.016.

[29] Jia G, Gardoni P. Stochastic life-cycle analysis: renewal-theory life-cycle analysis with state-dependent deterioration stochastic models. Struct Infrastruct Eng 2019;15:1001–14. https://doi.org/10.1080/15732479.2019.1590424.

[30] Stewart MG. Mechanical behaviour of pitting corrosion of flexural and shear reinforcement and its effect on structural reliability of corroding RC beams. Struct Saf 2009;31:19–30. https://doi.org/10.1016/j.strusafe.2007.12.001.

[31] Biondini F, Frangopol DM. Time-variant redundancy and failure times of deteriorating concrete structures considering multiple limit states. Struct Infrastruct Eng 2017;13:94–106. https://doi.org/10.1080/15732479.2016.1198403.

[32] Zhu W, François R, Cleland D, Coronelli D. Failure mode transitions of corroded deep beams exposed to marine environment for long period. Eng Struct 2015;96:66–77. https://doi.org/10.1016/j.engstruct.2015.04.004.

[33] Li J, Chen JB, Fan WL. The equivalent extreme-value event and evaluation of the structural system reliability. Struct Saf 2007;29:112–31. https://doi.org/10.1016/j.strusafe.2006.03.002.

[34] Stewart MG. Spatial and time-dependent reliability modelling of corrosion damage, safety and maintenance for reinforced concrete structures. Struct Infrastruct Eng 2012;8:607–19. https://doi.org/10.1080/15732479.2010.505379.

[35] Xiaoqun Wang, Ian H. Sloan. Low discrepancy sequences in high dimensions: How well are their projections distributed? J Comput Appl Math 2008;213:366–86.

[36] McKay MD, Beckman RJ, Conover WJ. A comparison of three methods for selecting values of input variables in the analysis of output from a computer code. Technometrics 1979;21:239–45. https://doi.org/10.1080/00401706.2000.10485979.

[37] Florian A. An efficient sampling scheme: Updated Latin Hypercube Sampling.

Probabilistic Eng Mech 1992;7:123–30. https://doi.org/10.1016/0266-8920(92)90015-A.

[38] Melchers RE. Importance sampling in structural systems. Struct Saf 1989;6:3–10. https://doi.org/10.1016/0167-4730(89)90003-9.

[39] Li J, Chen JB, Sun W, Peng Y. Advances of the probability density evolution method for nonlinear stochastic systems. Probabilistic Eng Mech 2012;28:132–42. https://doi.org/10.1016/j.probengmech.2011.08.019.

[40] Li J, Chen JB. Stochastic dynamics of structures. John Wiley & Sons; 2009. https://doi.org/10.1103/PhysRevE.82.041129.

[41] Dostupov BG, Pugachev VS. The equation to define a probability distribution, of the integral of a system of ordinary differential equations with randon parameters. Mat Sb 1957;18:620–30.

[42] Xu J, Chen J, Li J. Probability density evolution analysis of engineering structures via cubature points. Comput Mech 2012;50:135–56. https://doi.org/10.1007/s00466-011-0678-2.

[43] Fan WL. Time-dependent reliability analysis of structure with performance mutations based on probability density evolution method and its application. Gongcheng Lixue/Engineering Mech 2013;30. https://doi.org/10.6052/j.issn.1000-4750.2012.08.0627.

[44] Courant R, Friedrichs K, Lewy H. About the partial difference equations in mathematical physics (Über die partiellen Differenzengleichungen der mathematischen Physik). Math Ann 1928;100:32–74.

[45] Gu XL, Guo HY, Zhou B Bin, Zhang WP, Jiang C. Corrosion non-uniformity of steel bars and reliability of corroded RC beams. Eng Struct 2018;167:188–202. https://doi.org/10.1016/j.engstruct.2018.04.020.

[46] Cairns J, Plizzari GA, Du Y, Law DW, Franzoni C. Mechanical properties of corrosion-damaged reinforcement. ACI Mater J 2005;102-M29:256–64.

[47] Zhang WP, Song XB, Gu XL, Li SB. Tensile and fatigue behavior of corroded rebars.

Constr Build Mater 2012;34:409–17.
https://doi.org/10.1016/j.conbuildmat.2012.02.071.
[48] Torres-Acosta AA, Navarro-Gutierrez S, Terán-Guillén J, Terán-Guillénb J, Terán-Guillén J. Residual flexure capacity of corroded reinforced concrete beams. Eng Struct 2007;29:1145–52. https://doi.org/10.1016/j.engstruct.2006.07.018.
[49] Auyeung Y, Balaguru P, Chung L. Bond behavior of corroded reinforcement bars. ACI Struct J 2000;97:214–20. https://doi.org/10.14359/826.
[50] Zhang WP, Zhou BB, Gu XL, Dai HC. Probability distribution model for cross-sectional area of corroded reinforcing steel bars. J Mater Civ Eng 2014;26:822–32. https://doi.org/10.1061/(ASCE)MT.1943-5533.0000888.
[51] Conway JH, Sloane NJA. Sphere Packings, Lattices and Groups. vol. 290. 1999. https://doi.org/10.1007/978-1-4757-6568-7.
[52] Li J, Chen JB. The number theoretical method in response analysis of nonlinear stochastic structures. Comput Mech 2007;39:693–708. https://doi.org/10.1007/s00466-006-0054-9.
[53] Radović I, Sobol IM, Tichy RF. Quasi-Monte Carlo methods for numerical integration: Comparison of different low discrepancy sequences. Monte Carlo Methods Appl 1996;2:1–14. https://doi.org/10.1515/mcma.1996.2.1.1.
[54] Chen J, Yang J, Li J. A GF-discrepancy for point selection in stochastic seismic response analysis of structures with uncertain parameters. Struct Saf 2016;59:20–31. https://doi.org/10.1016/j.strusafe.2015.11.001.
[55] Jiang Z, Li J. High dimensional structural reliability with dimension reduction. Struct Saf 2017;69:35–46. https://doi.org/10.1016/j.strusafe.2017.07.007.
[56] Tao W, Li J. An Ensemble Evolution Numerical Method for Solving Generalized Density Evolution Equation. Probabilistic Eng Mech 2017;48:1–11. https://doi.org/10.1016/j.probengmech.2017.03.001.
[57] Bhargava K, Ghosh AK, Mori Y, Ramanujam S. Corrosion-induced bond strength degradation in reinforced concrete-Analytical and empirical models. Nucl Eng Des

2007;237:1140–57. https://doi.org/10.1016/j.nucengdes.2007.01.010.

[58] Bhargava K, Ghosh AK, Mori Y, Ramanujam S. Suggested Empirical Models for Corrosion-Induced Bond Degradation in Reinforced Concrete. J Struct Eng 2008;134:221–30. https://doi.org/10.1061/(asce)0733-9445(2008)134:2(221).

[59] CEB-FIP MC. Model code for concrete structures. Bull D'Information 1990.

[60] GB50010-2010, GB50010-2009, China National Standards. Code for Design of Concrete Structures. vol. Beijing. China: GB50010-2010; 2010.

[61] Wan Z, Chen J, Beer M. Pathways for Uncertainty Quantification through Stochastic Damage Constitutive Models of Concrete. 13th Int. Conf. Appl. Stat. Probab. Civ. Eng. ICASP13, 2019, p. 1–8.

Appendix

A.1 A review: Point evolution method and FDM for PDFM

The computational process of point evolution is introduced herein. First, the random space is divided into n_{sel} sub-domains [39], i.e. n_{sel} representative points. Denoting the number of random variables is d; each sub-domain can be represented by given vector $\boldsymbol{\theta}_a = [\theta_{a,1}, \theta_{a,2}, \ldots, \theta_{a,d}]^T$, $a = 1, 2, \ldots, n_{sel}$ and the probability-assigned p_a

$$p_a = \Pr\{\boldsymbol{\Theta} \in V_a\} = \int_{V_a} p_{\boldsymbol{\Theta}}(\boldsymbol{\theta})\, \mathrm{d}\boldsymbol{\theta}, a = 1, 2, ..., n_{sel} \tag{40}$$

where $p_{\boldsymbol{\Theta}}(\boldsymbol{\theta})$ is the joint PDF of random vector, $\boldsymbol{\Theta}$, and V_a is the Voronoi volume of the a-th subdomain Ω_a [51]. By using a low-discrepancy sequence (e.g. number-theoretical method (NTM) [52] or Sobol sequence [53]), uniform point set, $\mathbf{x}$, is acquired in terms of the number of random variables, d, and representative point, n_{sel}. Then, based on the distribution type of random variables in the target case, initial point set, $\boldsymbol{\Theta}$, can be acquired, in which each point $\theta_{q,a}$ (the q-th random variable and a-th representative point), can be yielded through

$$\theta_{q,a} = F_q^{-1}\left(x_{q,a}\right), q = 1, 2, ..., d, a = 1, 2, ..., n_{sel} \tag{41}$$

where $F_q^{-1}(\cdot)$ is the inverse cumulative distribution function of the q-th random variable. Then, the assign-probabilities, p_a, of each representative point can be computed through integration of Eq.(40). However, due to the high non-linearity of $F_q^{-1}(\cdot)$, the initial point set obtained through Eq.(41) is usually unacceptable, unless n_{sel} is very large [54]. Thus, it is necessary to refine the quality of the point set and rearrange it. In this study, Eq.(9) was used to obtain new point, $\theta'_{q,j}$ (the q-th random variable and j-th representative point) [54].

$$\theta'_{q,j} = F_q^{-1}\left\{\sum_{a=1}^{n_{sel}} p_a \cdot I\{\theta_{q,a} < \theta_{q,j}\} + 0.5 p_j\right\} \tag{42}$$

where $\theta_{q,j}$ is the initial q-th random variable in the j-th representative point, p_j is the assign-probability of the j-th representative point, and $I\{\cdot\}$ is an indicator function, which means that $I\{\cdot\} = 1$, if the condition is satisfied.

Then, the assign-probabilities, p_a, need to be recalculated with Eq.(40). Existing studies have proven that the above steps could significantly reduce the generalized F-discrepancy (GF-

878 discrepancy) D_{GF} of the point set (Eq. (43)), and improve its quality [54–56].

879
$$D_{GF}(\Theta)=\max_{1\le q\le d}\left\{\sup\left|F_{n_{sel},q}(\boldsymbol{\theta})-F_q(\boldsymbol{\theta})\right|\right\} \tag{43}$$

880 where $F_{nsel,q}(\cdot)$ and $F_q(\cdot)$ are the q-th marginal empirical and actual cumulative distribution
881 functions (CDF) of d-elements of the random vector, $\boldsymbol{\Theta}$.

882 Once the selection of the point set is done, integrating the GDEE, Eq.(8), on an arbitrary
883 sub-domain, Ω_a

884
$$\begin{aligned}&\int_{\Omega_a}\frac{\partial p_{G\boldsymbol{\Theta}}(g,\boldsymbol{\theta},t)}{\partial t}\mathrm{d}\boldsymbol{\theta}+\int_{\Omega_a}\dot{G}(\boldsymbol{\Theta},t)\frac{\partial p_{G\boldsymbol{\Theta}}(g,\boldsymbol{\theta},t)}{\partial g}\mathrm{d}\boldsymbol{\theta}\\&=\frac{\partial}{\partial t}\int_{\Omega_a}p_{G\boldsymbol{\Theta}}(g,\boldsymbol{\theta},t)\mathrm{d}\boldsymbol{\theta}+\dot{G}(\tilde{\boldsymbol{\theta}}_a,t)\frac{\partial}{\partial g}\int_{\Omega_a}p_{G\boldsymbol{\Theta}}(g,\boldsymbol{\theta},t)\mathrm{d}\boldsymbol{\theta}\\&=\frac{\partial p_G^a(g,t)}{\partial t}+\dot{G}(\tilde{\boldsymbol{\theta}}_a,t)\frac{\partial p_G^a(g,t)}{\partial g}=0,a=1,2,...,n_{sel}\end{aligned} \tag{44}$$

885 where $p^a{}_G(g, t)$ is the integration of $p_{G\boldsymbol{\Theta}}(g, \boldsymbol{\theta}, t)$ on Ω_a and $\dot{G}(\tilde{\boldsymbol{\theta}}_a,t)$ is the derivative function
886 of $\{G(\boldsymbol{\theta}, t), \boldsymbol{\theta}\in\Omega_a\}$, which is denoted as $\dot{G}(\boldsymbol{\theta}_a,t)$.

887 The finite difference method (FDM) is employed to solve Eq.(44) through the total
888 variation diminishing (TVD) scheme [40]

889
$$\begin{aligned}p_{k+1,j}^{[a]}&=p_{k,j}^{[a]}-\frac{1}{2}\left(\lambda v-|\lambda v|\right)\Delta p_{k,j+\frac{1}{2}}^{[a]}-\frac{1}{2}\left(\lambda v+|\lambda v|\right)\Delta p_{k,j-\frac{1}{2}}^{[a]}\\&-\frac{1}{2}\left(|\lambda v|-\lambda^2v^2\right)\left(\psi_{j+\frac{1}{2}}\Delta p_{k,j+\frac{1}{2}}^{[a]}-\psi_{j-\frac{1}{2}}\Delta p_{k,j-\frac{1}{2}}^{[a]}\right),a=1,2,...,n_{sel}\end{aligned} \tag{45}$$

890
$$v=\left[\dot{G}(\theta_a,t_k)+\dot{G}(\theta_a,t_{k+1})\right]/2 \tag{46}$$

891 where λ is the mesh ratio of time step Δt to space step Δx, $p_{k,j}^{[a]}$ denotes $p^a{}_G(g_j, t_k)$; $\Delta p_{k,j+\frac{1}{2}}^{[a]}$
892 and $\Delta p_{k,j-\frac{1}{2}}^{[a]}$ mean $p_{k,j+1}^{[a]}-p_{k,j}^{[a]}$ and $p_{k,j}^{[a]}-p_{k,j-1}^{[a]}$, respectively; $\psi_{j+\frac{1}{2}}$ and $\psi_{j-\frac{1}{2}}$ are the flux
893 limiters

894
$$\begin{aligned}\psi_{j+\frac{1}{2}}\left(r_{j+\frac{1}{2}}^{+},r_{j+\frac{1}{2}}^{-}\right)&=H(-v)\psi_0\left(r_{j+\frac{1}{2}}^{+}\right)+H(v)\psi_0\left(r_{j+\frac{1}{2}}^{-}\right),\\\psi_{j-\frac{1}{2}}\left(r_{j-\frac{1}{2}}^{+},r_{j-\frac{1}{2}}^{-}\right)&=H(-v)\psi_0\left(r_{j-\frac{1}{2}}^{+}\right)+H(v)\psi_0\left(r_{j-\frac{1}{2}}^{-}\right)\end{aligned} \tag{47}$$

$$r^{+}_{j+\frac{1}{2}}=\frac{p^{[a]}_{k,j+2}-p^{[a]}_{k,j+1}}{p^{[a]}_{k,j+1}-p^{[a]}_{k,j}},r^{-}_{j+\frac{1}{2}}=\frac{p^{[a]}_{k,j}-p^{[a]}_{k,j-1}}{p^{[a]}_{k,j+1}-p^{[a]}_{k,j}},r^{+}_{j-\frac{1}{2}}=\frac{p^{[a]}_{k,j+1}-p^{[a]}_{k,j}}{p^{[a]}_{k,j}-p^{[a]}_{k,j-1}},r^{-}_{j-\frac{1}{2}}=\frac{p^{[a]}_{k,j-1}-p^{[a]}_{k,j-2}}{p^{[a]}_{k,j}-p^{[a]}_{k,j-1}} \tag{48}$$

$$\psi_0(r)=\max(0,\min(2r,1),\min(r,2)) \tag{49}$$

Additionally, the absorbing boundary condition in Eq.(5) is imposed to get the residual PDF $p^{a*}{}_G(g, t)$, a = 1, 2, … , n_{sel} is calculated, $p^{*}{}_G(g, t)$ could be obtained by summing all $p^{a*}{}_G(g, t)$ Eq.(50), and $P_f(t)$ is calculated by Eq.(6).

$$p^{*}_{G}\left(g,t\right)=\sum_{a=1}^{n_{sel}}p^{a*}_{G}(g,t) \tag{50}$$

A.2 Flexural capacity of corroded RC beam considering bond strength loss

The prediction of bond degradation is based on the model proposed by Bhargava [57, 58]. Assuming the ultimate bond strength $T_{bux,j,i}$ of the arbitrary *j*-th corroded steel bar at *i*-element is higher than the critical bond failure strength $T_{ub,rqd}$, the flexural capacity of the *i*-th element $M_{ux,i}$ can be computed as

$$T_{ubx,j,i}=T_{\max 0}\cdot R_{bond}\left(1-\frac{A_{\min,j,i}}{A_{s0}}\right) \tag{51}$$

$$R_{bond}(n_s)=\begin{cases}1, n_s\le 1.5\%\\ 1.346e^{-0.198n_s}\cdot H\left[R_{bond}(n_s)-0.02\right]\\ 0.02\cdot\left\{1-H\left[R_{bond}(n_s)-0.02\right]\right\}, n_s>1.5\%\end{cases} \tag{52}$$

$$T_{ub,rqd}=\frac{f_{y0}D_{s0}}{4l_d} \tag{53}$$

where T_{max0} is the bond strength between an uncorroded steel bar and surrounding concrete, which could be calculated by [59]

$$T_{\max 0}=2.0\cdot(f_c)^{0.5} \tag{54}$$

and l_d is the development length of bond strength and can be calculated as [60]

$$l_d=\alpha_s\frac{f_{yd}}{f_t}D_{s0} \tag{55}$$

where α_s is the shape coefficient (0.14 for a deformed bar and 0.16 for a plain bar [60]) and f_t is

915 the tensile strength of concrete.

916 A relationship between tensile strength, f_t, and compressive strength, f_c, for concrete is
917 used to evaluate f_t [61]

918 $$f_t = 0.26 f_c^{2/3} \tag{56}$$

919 If $T_{bux,j,i}$ is lower than $T_{ub,rqd}$, anchorage failure occurs due to insufficient bond strength and
920 tensile force; $F_{stx,j,i}$ of the j-th corroded steel bar at the i-th element, is governed by ultimate
921 bond strength rather than its yielding strength.

922 $$F_{stx,j,i}(t) = \pi D_{s,j,i}(t) l_d T_{ubx,j,i} \tag{57}$$

923 where, $D_{s,j,i}(t)$ is the equivalent diameter of the j-th steel bar at the i-th element, which is
924 calculated by

925 $$D_s(t) = \sqrt{\frac{4}{\pi} A_{\min,j,i}(t)} \tag{58}$$

926 Supposing the deformation of concrete at the steel bar surface is caused by plastic
927 deformation within the plastic equivalent region (L_{eq}), the strain compatibility of corroded RC
928 beam can be expressed as

929 $$\frac{\bar{\varepsilon}_{stx,i}}{\varepsilon_{ccx,i}} = \left[1 - \left(1 - \frac{\sum_{j=1}^{n} T_{ubx.j,i}}{n T_{ub0}}\right)\left(1 - \frac{L_{eq,i}}{l_d}\right)\right] \frac{h_0 - Y_{x,i}}{Y_{x,i}} \tag{59}$$

930 $$L_{eq,i} = 9.3 Y_{x,i} \tag{60}$$

931 where, $Y_{x,i}$ is the neutral axis depth of the i-th element and T_{ub0} is the bond strength of the
932 uncorroded steel bar. The average strain of the steel reinforcing bar, $\overline{\varepsilon_{stx.i}}$, at the i-th element
933 can be calculated by

934 $$\bar{\varepsilon}_{stx,i} = \frac{1}{n} \sum_{j=1}^{n} \frac{F_{stx,j,i}}{E_{st} A_{\min,j,i}} \tag{61}$$

935 where, E_{st} is the elastic modulus of the corroded steel bar; E_{st} remains unchanged but slightly
936 fluctuates with the degree of corrosion [45].

937 The elastic modulus of the corroded steel bar, E_{st}, is regarded as a random variable herein.

When anchorage failure occurs before the yielding of the steel bar, the tensile stress of the corroded steel bar can be computed using Eq.(57) and then $Y_{x,i}$ and M_i can be obtained as

$$Y_{x,i} = \frac{\sum_{i=1}^{n_{st}} F_{stx,j,i}}{\eta \lambda f_c b} \tag{62}$$

$$M_i = F_{ccx,i}\left(h_0 - 0.5\lambda Y_x\right) \tag{63}$$

where $F_{ccx,i} = \eta\,\lambda\, f_c Y_{x,i}$ (η and λ are factors 1 and 0.8, respectively) and is the compressive force of the cross-section.

When the steel bar yields before anchorage failure, its residual yield strength governs the tensile force of the corroded steel bar. If the tensile bar yields and the concrete crushes before anchorage failure, the strain of the steel bar is governed by the concrete crushing. Given $\varepsilon_{ccx,i}$ and ε_{cc}, the average strain of the steel reinforcing bar, $\overline{\varepsilon_{stx.i}}$, can be calculated by Eq.(59). Then, $F_{stx,j,i}$ and M_i can be computed by Eqs. (64) and (63), respectively.

$$F_{stx,j,i} = E_{st}\overline{\varepsilon}_{stx,i}A_{\min,j,i} \tag{64}$$

The bisection method could be applied to solve $Y_{x,i}$ to satisfy Eqs.(59), (62), and (64). Apart from that, considering both the brittle parallel system and the degradation of bond strength, $\sum_{j=1}^{n} T_{ubx.j,i}$ in Eq.(59) and $\sum_{i=1}^{n_{st}} F_{stx,j,i}$ in Eq. (62) can also be computed by Eq. (38).